






RESEARCH ARTICLE

Pathways linking aging and atheroprotection in *Mif*-deficient atherosclerotic mice

Christine Krammer¹ | Bishan Yang¹ | Sabrina Reichl¹ | Simon Besson-Girard^{2,3}  | Hao Ji² | Verena Bolini¹ | Corinna Schulte⁴ | Heidi Noels^{4,5} | Kai Schlepckow⁶ | Georg Jocher⁶ | Georg Werner⁷ | Michael Willem⁷ | Omar El Bounkari¹  | Aphrodite Kapurniotu⁸  | Ozgun Gokce^{2,9} | Christian Weber^{5,9,10,11} | Sarajo Mohanta¹⁰  | Jürgen Bernhagen^{1,9,11} 

¹Division of Vascular Biology, Institute for Stroke and Dementia Research (ISD), LMU University Hospital, Ludwig-Maximilians-University (LMU), Munich, Germany

²Systems Neuroscience Laboratory, Institute for Stroke and Dementia Research (ISD), LMU University Hospital, Munich, Germany

³Graduate School of Systemic Neurosciences (GSN), LMU Munich, Planegg-Martinsried, Germany

⁴Institute for Molecular Cardiovascular Research (IMCAR), University Hospital Aachen, Rhenish-Westphalian Technical University (RWTH) Aachen University, Aachen, Germany

⁵Cardiovascular Research Institute Maastricht (CARIM), Maastricht University, Maastricht, The Netherlands

⁶German Center for Neurodegenerative Diseases (DZNE), Munich, Germany

⁷Metabolic Biochemistry, Biomedical Center (BMC), Faculty of Medicine, Ludwig-Maximilians-Universität München, Munich, Germany

⁸Division of Peptide Biochemistry, TUM School of Life Sciences, Technical University of Munich (TUM), Munich, Germany

⁹Munich Cluster for Systems Neurology (SyNergy), Munich, Germany

¹⁰Institute for Cardiovascular Prevention, LMU University Hospital, Ludwig-Maximilians-University (LMU), Munich, Germany

¹¹Munich Heart Alliance, Munich, Germany

Correspondence

Jürgen Bernhagen, Institute for Stroke and Dementia Research (ISD), LMU University Hospital (LMU Klinikum), Ludwig-Maximilians-Universität (LMU) München, Feodor-Lynen-Straße

Abstract

Atherosclerosis is a chronic inflammatory condition of our arteries and the main underlying pathology of myocardial infarction and stroke. The pathogenesis is age-dependent, but the links between disease progression, age, and atherogenic

Abbreviations: ACKs, atypical chemokines; *Aldh6a1*, aldehyde dehydrogenase 6 family member A1; *ApoE*, Apolipoprotein E; ATLOs, artery tertiary lymphoid organs; BAT, brown adipose tissue; BCA, brachiocephalic artery; BM, bone marrow; CAD, coronary artery disease; CCL2 or 7 or 11, C-C motif chemokine ligand 2 or 7 or 11; CD3 or 4, cluster of differentiation 3 or 4; *Col4a4*, type IV collagen; *Cpne7*, copine 7; CSF-1, colony stimulating factor 1; CSF1R, colony stimulating factor 1 receptor; CXCL1 or 2 or 8 or 13, C-X-C motif chemokine ligand 1 or 2 or 8 or 13; CXCR2 or 4, C-X-C motif chemokine receptor 2 or 4; CVDs, cardiovascular diseases; EDTA, ethylene diamine tetra-acetic acid; ELISA, enzyme-linked immunosorbent assay; FALCs, fat-associated lymphoid clusters; FDCs, follicular dendritic cells; *Foxp3*, forkhead box p3; GC, germinal center; HEVs, high-endothelial venules; HFD, high fat diet; IL-1 β , interleukin-1 β ; *Ifn- γ* , interferon gamma; *Il-6 or -10 or -34*, interleukin-6 or -10 or -34; *Jaml*, junctional adhesion molecule-like; Ldlr, low density lipoprotein receptor; LNs, lymph nodes; LYVE-1, lymphatic vessel endothelial hyaluronan receptor-1; MIF, macrophage migration inhibitory factor; NASH, non-alcoholic steatohepatitis; oxLDL, low-density lipoprotein; PBS, phosphate-buffered saline; *Plin1 or 4*, perilipin 1 or 4; PFA, paraformaldehyde; PNA_d, peripheral node addressin; PVAT, perivascular adipose tissue; RBC, red blood cell; *Rnd1*, Rho family GTPase 1; SMCs, smooth muscle cells; SLO, secondary lymphoid organ; T2D, type 2 diabetes; TNF- α , tumor necrosis factor alpha; *Tnnt3*, troponin T3; Trem2, triggering receptor expressed on myeloid cells 2; *Thrsp*, thyroid hormone-inducible hepatic protein; WAT, white adipose tissue.

Christine Krammer and Bishan Yang contributed equally to this work.

This is an open access article under the terms of the [Creative Commons Attribution-NonCommercial](https://creativecommons.org/licenses/by-nc/4.0/) License, which permits use, distribution and reproduction in any medium, provided the original work is properly cited and is not used for commercial purposes.

© 2023 The Authors. *The FASEB Journal* published by Wiley Periodicals LLC on behalf of Federation of American Societies for Experimental Biology.

17, Munich 81377, Germany.
Email: juergen.bernhagen@med.uni-muenchen.de

Funding information

Deutsche Forschungsgemeinschaft (DFG), Grant/Award Number: SFB1123, EXC 2145 SyNergy-ID 390857198 and SFB-TRR219-M05

cytokines and chemokines are incompletely understood. Here, we studied the chemokine-like inflammatory cytokine macrophage migration inhibitory factor (MIF) in atherogenic *Apoe*^{-/-} mice across different stages of aging and cholesterol-rich high-fat diet (HFD). MIF promotes atherosclerosis by mediating leukocyte recruitment, lesional inflammation, and suppressing atheroprotective B cells. However, links between MIF and advanced atherosclerosis across aging have not been systematically explored. We compared effects of global *Mif*-gene deficiency in 30-, 42-, and 48-week-old *Apoe*^{-/-} mice on HFD for 24, 36, or 42 weeks, respectively, and in 52-week-old mice on a 6-week HFD. *Mif*-deficient mice exhibited reduced atherosclerotic lesions in the 30/24- and 42/36-week-old groups, but atheroprotection, which in the applied *Apoe*^{-/-} model was limited to lesions in the brachiocephalic artery and abdominal aorta, was not detected in the 48/42- and 52/6-week-old groups. This suggested that atheroprotection afforded by global *Mif*-gene deletion differs across aging stages and atherogenic diet duration. To characterize this phenotype and study the underlying mechanisms, we determined immune cells in the periphery and vascular lesions, obtained a multiplex cytokine/chemokine profile, and compared the transcriptome between the age-related phenotypes. We found that *Mif* deficiency promotes lesional macrophage and T-cell counts in younger but not aged mice, with subgroup analysis pointing toward a role for Trem2⁺ macrophages. The transcriptomic analysis identified pronounced MIF- and aging-dependent changes in pathways predominantly related to lipid synthesis and metabolism, lipid storage, and brown fat cell differentiation, as well as immunity, and atherosclerosis-relevant enriched genes such as *Plin1*, *Ldlr*, *Cpne7*, or *Il34*, hinting toward effects on lesional lipids, foamy macrophages, and immune cells. Moreover, *Mif*-deficient aged mice exhibited a distinct plasma cytokine/chemokine signature consistent with the notion that mediators known to drive inflamm'aging are either not downregulated or even upregulated in *Mif*-deficient aged mice compared with the corresponding younger ones. Lastly, *Mif* deficiency favored formation of lymphocyte-rich peri-adventitial leukocyte clusters. While the causative contributions of these mechanistic pillars and their interplay will be subject to future scrutiny, our study suggests that atheroprotection due to global *Mif*-gene deficiency in atherogenic *Apoe*^{-/-} mice is reduced upon advanced aging and identifies previously unrecognized cellular and molecular targets that could explain this phenotype shift. These observations enhance our understanding of inflamm'aging and MIF pathways in atherosclerosis and may have implications for translational MIF-directed strategies.

KEYWORDS

aging, artery tertiary lymphoid organ, atherosclerosis, atypical chemokines, chemokines, MIF

1 | INTRODUCTION

Cardiovascular diseases (CVDs) such as myocardial infarction or ischemic stroke are the main underlying causes of death worldwide and incidence risk has steadily increased over the last decades. Disease pathology has

been associated with multiple comorbidities and risk factors such as hypertension, type 2 diabetes (T2D), or metabolic syndrome, which are further impaired by diet and lifestyle changes and increasingly manifest in an aging population.^{1,2} Atherosclerosis is a lipid-triggered chronic inflammatory condition of the arterial vasculature and is

the main underlying pathology of CVDs. Atherosclerosis progressively develops over years and decades and is typically clinically symptomatic in later adulthood. Triggered by endothelial dysfunction and oxidized low-density lipoprotein (oxLDL) uptake, lipid and inflammatory cell deposits in the arterial vessel wall drive the formation of atheromatous lesions. Lesion formation involves oxLDL-mediated foam cell formation and leukocyte infiltration, a process orchestrated by endothelial-deposited chemokines and their receptors expressed on infiltrating inflammatory cells. Cytokines and chemokines promote and perpetuate vascular inflammation through a variety of pathways. Together, this results in increased atherogenic leukocyte recruitment, atherosclerotic wall remodeling, necrotic core formation, plaque destabilization, and rupture, resulting in atherothrombosis with adverse clinical outcomes such as myocardial infarction or stroke.³⁻⁶

In addition to classical atherogenic chemokines such as CCL2, CXCL1/8, or CXCL2, atypical chemokines (ACKs) have emerged as players in the atherogenic inflammatory cascade. Atypical chemokines have chemokine-like properties and engage in high-affinity interactions with classical chemokine receptors, but lack classifying structural features of bona fide chemokines such as an N-terminal CC- or CXC-motif.⁷ Macrophage migration inhibitory factor (MIF) is an evolutionarily conserved pleiotropic inflammatory cytokine and prototypical ACK with a proatherogenic activity spectrum. MIF is overexpressed in human carotid artery plaques⁸ and circulating MIF levels have been associated with coronary artery disease (CAD), suggesting a critical role for MIF in CVDs.⁹⁻¹¹ MIF secretion mainly occurs from monocytes, T cells, endothelial cells, smooth muscle cells (SMCs), and platelets,^{7,12} and its expression is upregulated by atherogenic stimuli such as inflammatory cytokines, oxLDL, or hypoxia.^{9,13} The CATT₆₋₈ MIF promoter polymorphism is associated with higher MIF expression in human inflammatory and autoimmune diseases and an increased susceptibility for carotid artery atherosclerosis (CAA).¹⁴⁻¹⁷ MIF signals through its cognate receptor CD74, but its proatherogenic activities are mainly mediated by noncognate signaling through the chemokine receptors CXCR2 and CXCR4. This drives the atherogenic recruitment of monocytes, neutrophils, T cells, and platelets,^{13,17,18} and promotes foam cell formation and vascular chemokine and adhesion molecule expression.^{8,19,20}

In vivo models of atherosclerosis suggest a causal role of MIF in atherosclerosis. *Mif*-gene deletion in hyperlipidemic *Ldl receptor*-deficient (*Ldlr*^{-/-}) mice^{18,21} or antibody-mediated blockade of MIF in *Apolipoprotein e*-deficient (*ApoE*^{-/-}) mice on a Western-type high-fat diet (HFD)^{20,22} lead to decreased luminal monocyte adhesion, lower plaque macrophage counts, attenuated lesion

formation, and increased plaque stability. More recently, Schmitz et al.²³ investigated *Mif*-gene deficiency in HFD-fed *ApoE*^{-/-} mice and revealed a site-specific atheroprotective phenotype in the brachiocephalic artery (BCA) and abdominal aorta, whereas other regions of the vascular bed were not affected.

In the *ApoE*^{-/-} mouse model of atherosclerosis, the development of advanced atheromatous plaques is typically studied in 12- to 24-week HFD feeding regimens,²⁴ but this and similar models do not fully mirror the advanced and late-stage vessel phenotypes and clinical manifestations observed in humans. Atherosclerotic mice at an advanced age of >32 weeks, which would be equivalent to an age span of >50 years in humans (<https://www.jax.org/research-and-faculty/research-labs/the-harrison-lab/gerontology/life-span-as-a-biomarker>),²⁵ have been investigated rather rarely. Furthermore, while studies on the impact of aging in atherosclerosis have identified contributing factors such as dysregulated inflammatory cytokines and chemokines or vascular mitochondrial dysfunction (also referred to as inflamm'aging),²⁶ the underlying mechanisms and details of their interplay with disease progression have remained incompletely understood. Moreover, adventitial B- and T-lymphocyte-rich leukocyte clusters, termed artery tertiary lymphoid organs (ATLOs), have emerged as age-dependent atherosclerosis-associated structures with disease-modulating activity.²⁷⁻²⁹ They are typically observed in 52- to 78-week-old *ApoE*^{-/-} mice,²⁷ and have also been detected in patients with CAD, but not much is currently known about their disease mechanism.³⁰ Overall, these observations highlight the link between aging and the dysregulation of the immune and inflammatory response in atherosclerosis.

Because MIF has not been studied in the context of aging, we here sought to characterize age-related effects of global *Mif*-gene deletion in advanced stages of atherosclerosis. We compared lesion phenotypes, leukocyte profiles, transcriptomic signatures, and inflammatory cytokine/chemokine profiles between *Mif*^{-/-} *ApoE*^{-/-} and *ApoE*^{-/-} mice that were on HFD for 24, 36, and 42 weeks, corresponding to an age of 30, 42, and 48 weeks, respectively, as well as in 52-week-old mice on HFD for 6 weeks. These age/HFD groups are hereinafter termed the 30/24-, 42/36-, 48/42-, and 52/6-week groups. Furthermore, peri-adventitial cell clusters and anti-oxLDL antibodies were analyzed. We confirm that global *Mif* deficiency in *ApoE*^{-/-} mice on HFD for 24 weeks confers atheroprotection and that atherosclerotic lesion reduction in *Mif*-deficient mice is restricted to the BCA and abdominal aorta in *ApoE*^{-/-} mice. Notably, the atheroprotective effect was reduced in the aged 48/42- and 52/6-week groups, most pronounced in the abdominal aorta. This was accompanied by MIF- and age-dependent changes in plaque immune cells, transcriptomic signatures,

the cytokine/chemokine profile, and peri-adventitial cell clusters. Together, our study for the first time reveals age-dependent functions of the atypical chemokine MIF in atherosclerotic pathology and suggests that a combination of mechanisms could account for reduced atheroprotection in *Mif*-deleted aged atherogenic *Apoe*^{-/-} mice.

2 | MATERIALS AND METHODS

2.1 | Chemicals, buffers, and miscellaneous reagents

Miscellaneous reagents were purchased from Sigma-Aldrich/Merck (Darmstadt, Germany), VWR International GmbH (Darmstadt, Germany), Carl Roth GmbH (Karlsruhe, Germany), and Ratiopharm (Ulm, Germany) and were of the highest purity degree available.

2.2 | Mice

Atherosclerosis-prone *Apolipoprotein*-deficient (*Apoe*^{-/-}) mice and *Apoe*^{-/-}*Mif*^{-/-} mice were in the C57BL/6-J background. *Apoe*^{-/-} mice were initially obtained from Charles River Laboratories (Sulzfeld, Germany) and were backcrossed within the animal facility of the Center for Stroke and Dementia Research (CSD). Global *Mif*-gene-deficient mice (*Mif*^{-/-}) were generated by Dr. Fingerle-Rowson and Prof. Richard Bucala and have been reported on before.^{23,31} For the generation of *Mif*^{-/-}*Apoe*^{-/-} mice, *Mif*^{-/-} mice were backcrossed with *Apoe*^{-/-} mice for at least 10 generations. Mice were housed and bred under standardized and specific pathogen-free conditions in the animal facility of the CSD in Munich, with free access to food and water. Animal experiments were approved by the local authorities (animal ethics approval ROB-55.2-2532. Vet_02-18-040) and were performed according to the German animal protection law. Animals were sacrificed under anesthesia with a mixture of midazolam (5 mg/ml), medetomidine, and fentanyl (MMF).

2.3 | Western-type high-fat diet (HFD)

Female animals received a regular chow diet (SNIFF Spezialdiäten GmbH, Soest, Germany) until 6 weeks of age and then were subjected to a high-cholesterol ("Western type") diet (HFD) containing 0.2% cholesterol and 21.2% total fat (TD88137, SNIFF Spezialdiäten GmbH, Soest, Germany) for an additional 24, 36, or 42 weeks. Mice aged 52 weeks received the HFD only in the last 6 weeks before the end of the experiment.

2.4 | Isolation of blood, organs, and vessels

Blood was collected by cardiac puncture into ethylene diamine tetra-acetic acid (EDTA)-containing tubes (Sarstedt, Nümbrecht, Germany), and hematologic parameters were subsequently analyzed using the Scil Vet aBCA Plus+ Blood Analyzer (Scil Animal Care Company GmbH, Viernheim, Germany). For plasma preparation, the blood was centrifuged at 400 g for 15 min at 4°C. Plasma samples were immediately frozen in liquid nitrogen and stored at -80°C. The circulation was rinsed with 15 ml of perfusion solution (100 U/ml heparin, 10 mM EDTA in phosphate-buffered saline (PBS), pH 7.4) followed by 15 ml of PBS.

Single-cell suspensions were generated from spleen, lymph nodes (LNs), and bone marrow (BM) of femur and tibia by filtering the cells through a 40 µm cell strainer (Corning, Sigma-Aldrich/Merck). After red blood cell (RBC) lysis using RBC lysis buffer (BioLegend, Koblenz, Germany), cells were washed in PBS and used for subsequent analysis. Different parts of the vascular bed, including the BCA and aortic root, were isolated and embedded in Tissue-Tek® O.C.T.™ compound (Sakura Finetek, Staufen, Germany). The embedded tissues were stored at -80°C until preparation of 5 µm thick serial cryosections. The whole aorta was excised, pinned onto a slide, and fixed overnight in 1% paraformaldehyde (PFA) at 4°C. The next day, the aorta was removed from surrounding fat and *en face* preparations were generated. The adventitia was removed, and the aorta pinned with the endothelium pointing upward. The *en face*-prepared vessel was again fixed in 4% PFA overnight and then applied to subsequent analyses.

2.5 | Flow cytometric analysis

Flow cytometric analysis was performed to analyze the immune cell content (CD8⁺ T cells: CD45⁺CD3e⁺CD8a⁺, CD4⁺ T cells: CD45⁺CD3e⁺CD4⁺, monocytes: CD45⁺CD11b⁺CD115⁺, neutrophils: CD45⁺CD11b⁺Ly6G⁺, B cells: CD45⁺CD19⁺) of different organs including BM, spleen, LN, and blood, using a BD FACSVerser™ instrument with a 3-laser, 8-color (4-2-2) configuration (BD Bioscience, Heidelberg, Germany). The system automatically adjusts spillover values for the compensation of standard fluorochromes. Cells were stained with fluorescently labeled antibodies directed against cell-specific surface marker for 30 min on ice in the dark (anti-mouse CD45-APC/Cy7, #103116, BioLegend; anti-mouse CD45-FITC, #FAB114F, R&D Systems, Wiesbaden-Nordenstadt, Germany; anti-mouse CD3e-FITC, #130-119-758, Miltenyi Biotech, Bergisch Gladbach, Germany; anti-mouse

CD4-PE, #130-102-619, Miltenyi Biotech; anti-mouse CD8a-PE-Cy7, #25-4321-82, Thermo Fisher Scientific, Darmstadt, Germany; anti-mouse CD19-PerCP-Cy5.5, #115534, BioLegend; anti-mouse CD11b-FITC, #130-081-201, Miltenyi Biotech; anti-mouse CD115-PE, #12-1152-82, Thermo Fisher Scientific; anti-mouse Ly6G-PerCP-Cy5.5, #45-5931-80, Thermo Fisher Scientific). The antibodies were diluted 1:100 in FACS staining buffer (0.5% bovine serum albumin (BSA)/PBS, pH 7.4). Afterward, the cells were washed with FACS buffer and centrifuged for 5 min at 300g and 4°C and flow cytometric analysis was performed. For control, cells were stained with respective isotype control antibodies purchased from BioLegend or R&D Systems (rat IgG2b, κ -APC/Cy7, rat IgG2b, κ -FITC, rat IgG2a, κ -PE, rat IgG2b, κ -PerCP/Cy5.5, rat IgG2a, κ -PerCP/Cy5.5, rat IgG2b, κ -PE, rat IgG2a, κ -PE/Cy7) or REA control antibodies (REA Control (I)-FITC, Miltenyi Biotech). Results were analyzed by FlowJo software (Tree star, USA) and presented as dot plots at a logarithmic scale.

2.6 | Flow cytometric analysis of proliferating Trem2⁺ bone marrow-derived macrophages

Flow cytometric analysis of proliferating Trem2⁺ cells was performed on preparations of bone marrow-derived macrophages (BMDMs) isolated from 24- and 42-week HFD-fed *ApoE*^{-/-} and *Mif*^{-/-}*ApoE*^{-/-} mice. BMDMs were isolated by an established procedure following a previously described protocol.³² Briefly, bone marrow cells were flushed and isolated from tibia and femur from the above mice, followed by differentiating the cells with 20 ng/ml murine M-CSF for 7 days. Afterward, differentiated BMDMs were labeled overnight with ethynyl deoxyuridine (Edu) (Click-iT™ Edu Alexa Fluor™ 488 Flow Cytometry Assay Kit, C10425, Thermo Fisher). For analysis, the BD FACSVerser™ instrument as described above was used, except that the biotinylated anti-mouse Trem2 monoclonal antibody 4D9³³ was used as primary antibody and APC-fluorescently labeled streptavidin (#17-4317-82, ThermoFisher Scientific) and AF488 fluorescent dye picolyl azide (Click-iT™ Edu Alexa Fluor™ 488 Flow Cytometry Assay Kit, C10425, Thermo Fisher Scientific) for detection. For isotype control, cells were stained with biotinylated rat IgG instead of the biotinylated anti-mouse Trem2 antibody.

2.7 | Plasma anti-oxLDL antibody titer

Plasma anti-oxLDL antibody levels were measured in Nunc MaxiSorp™ 96-well plates (Thermo Fisher

Scientific) coated with 1 μ g/ml oxLDL (Thermo Fisher Scientific) diluted in carbonate buffer (34.8 mM NaHCO₃, 15 mM Na₂CO₃ in double-distilled (dd)H₂O). After coating for 1 h at 37°C, plates were washed three times with 100 μ l of washing/blocking solution (2% BSA in PBS) and blocked for 1 h at 37°C. Next, 50 μ l plasma diluted 1:100 in washing/blocking solution was added per well and incubated for 1 h at 37°C. The plates were washed again and 50 μ l of horseradish-peroxidase (HRP)-labeled antibodies against IgG (# ab6789, Abcam, Berlin, Germany) and IgM (#62-6820, Thermo Fisher Scientific) diluted 1:500 in washing/blocking solution were applied and incubated for 1 h at 37°C. Following additional washing steps, the assay was developed by adding 100 μ l Pierce™ 3,3',5,5'-tetramethylbenzidine (TMB) substrate solution (Thermo Fisher Scientific) for 5 min and the reaction was stopped by applying 50 μ l stop solution (0.5 M H₂SO₄ in ddH₂O). Measurements were performed using an EnSpire Multimode Plate Reader (PerkinElmer, Hamburg, Germany) at 450 nm.

2.8 | Plaque morphometry, immunofluorescence, en face staining of aorta, and plaque lipids

2.8.1 | Immunofluorescence of brachiocephalic artery

Immunohistochemistry was performed on 5 μ m thick cryosections of the BCA. The sections were fixed with precooled acetone at 4°C for 6 min and air-dried at room temperature (RT) for 30 min, following rehydration in PBS for 10 min. Next, the sections were blocked for 30 min with blocking solution (5% donkey/goat serum, 1% BSA in PBS, pH 7.4). Next, the sections were incubated with the primary antibodies diluted in blocking solution at 4°C overnight. The following primary antibodies were applied: rat anti-mouse CD45R/B220 (1:100, #557390, BD Biosciences), rat anti-mouse CD68 (1:100, #MCA1957GA, Bio-Rad, Puchheim, Germany), hamster anti-mouse CD3e (1:100, #553058, BD Biosciences), mouse anti-human/mouse SMA-Cy3 (1:200, #C6198, Sigma-Aldrich), rat anti-mouse CD35 (1:100, #558768, BD Biosciences), rat anti-mouse PNA^d (1:50, #553863, BD Biosciences), rabbit anti-mouse collagen IV (1:500, #2150-1470, Bio-Rad), rat anti-mouse ER-TR7 (1:500, #ab51824, Abcam), rabbit anti-mouse Lyve1 (1:500, #DP35135P, Acris Antibody GmbH, Herford, Germany), sheep anti-mouse Trem2 (1:50, #AF1729, R&D Systems), and rabbit anti-mouse Ki67 (1:200, #9129T, Cell Signaling). Afterward, sections were washed in PBS and incubated for 1 h at RT with the respective secondary

antibodies diluted in blocking solution. The following secondary antibodies were used: donkey anti-rat-Cy5 (1:300, Jackson ImmunoResearch, Hamburg, Germany, #712-175-153), goat anti-rat-AF488 (1:500, #A-11006, Thermo Fisher Scientific), goat anti-hamster-Cy3 (1:300, #127-165-160, Jackson ImmunoResearch), goat anti-rat(IgM)-Cy5 (1:500, #A21247, Thermo Fisher Scientific), donkey anti-rabbit-Cy3 (1:500, #711-165-152, Jackson ImmunoResearch), donkey anti-rat-Cy3 (1:300, #712-166-153, Jackson ImmunoResearch), donkey anti-sheep-AF555 (1:500, ab150178, Abcam), donkey anti-sheep-AF647 (1:500, ab150179, Abcam), and goat anti-rabbit-AF647 (1:300, #A21245, Thermo Fisher Scientific). DAPI was used as nuclear counterstain. Afterward, sections were washed and mounted with Fluoromount™ aqueous mounting medium (Sigma-Aldrich/Merck). Images were recorded with a DMi8 fluorescent microscope or a TCS SP5II MP confocal microscope (Leica Microsystems, Wetzlar, Germany), and analyses were performed using ImageJ software.

2.8.2 | Oil-Red-O staining of aortic root

For the quantification of lesion formation in the aortic root, Oil-Red-O (ORO) stainings were performed on 5 μm thick cryosections. First, the slides were air-dried for 5 min following rehydration in PBS for 2 min. Next, lipids were stained with ORO solution (0.5% in propylene glycol, Sigma-Aldrich/Merck) at 37°C for 45 min. The slides were shortly washed with running tap water, and nuclear counterstain was performed using hematoxylin. The slides were air-dried and mounted with Kaiser's glycerin gelatine mounting media (Carl Roth, Karlsruhe, Germany). Images were taken with the DMi8 fluorescent microscope, and lesion quantification performed using ImageJ software. Per mouse, 12 serial sections with a distance of 50 μm between each other, were stained, and mean values calculated.

2.8.3 | Oil-Red-O (en face) staining of aorta

Oil-Red-O stainings of the aorta including aortic arch as well as abdominal and thoracic aorta were performed after *en face* preparation and fixation in 4% PFA. The tissue was stained for 30 min in ORO solution (0.5% in isopropanol, Sigma-Aldrich/Merck) at RT. Next, aortas were washed in 60% isopropanol until unspecific ORO-derived staining was removed from the endothelium. The aortas were rinsed briefly with running tap water before mounting in Kaiser's glycerin gelatine mounting media. Tifescan images were acquired with the DMi8

fluorescent microscope. The lesions were quantified via Image J software and depicted as percentage of total aortic surface.

2.8.4 | Hematoxylin–eosin staining of brachiocephalic artery

Hematoxylin–eosin (H&E) staining was performed for lesion quantification of the BCA. The slides were air-dried at RT for 30 min and rehydrated with PBS for 2 min. Next, nuclei were stained with Mayer's hematoxylin solution (Sigma-Aldrich/Merck) for 15 min at RT. Then, the slides were washed in running tap water for 10 min before staining with Eosin G-solution for 10 s and dehydration by two changes of 95% ethanol, 100% ethanol, and xylene (2 min each). After air-drying, the slides were mounted using a VECTASHIELD® antifade mounting medium (Vector Laboratories). Images were taken with a Leica DMi8 or a Leica DM6 B fluorescent microscope. The lesion size was quantified using ImageJ software and is depicted as ratio of total inner vessel area. Per mouse, 12 sections with a distance of 50 μm between them were stained and the mean values calculated.

2.9 | RT-qPCR-based mRNA expression analysis

Messenger RNA expression levels of cytokines/chemokines *Mif*, *Il-1β*, *Ifn-γ*, *Il-6*, and *Cxcl1*, T-cell markers *Cd3* (all T cells) and *FoxP3* (Tregs), as well as adipokines leptin and adiponectin were quantified by RT-qPCR from various frozen tissues (i.e., spleen, liver, total aorta, and epididymal white adipose tissue (WAT)) as specified in the Results and Figures.

2.9.1 | TRIzol-based RNA isolation

For the analysis of MIF mRNA levels, RNA was extracted from frozen tissues using a TRIzol™-based protocol. First, tissue was homogenized in 1 ml of TRIzol™ reagent (Thermo Fisher Scientific) using stainless steel beads (5 mm mean diameter) and a TissueLyser LT adapter (Qiagen, Hilden, Germany) for 5 min at 50 Hz. Afterward, tissue lysates were incubated for 5 min to permit complete dissociation of nucleoprotein complexes. After adding 200 μl of chloroform and incubation for 3 min, the solution was centrifugation for 15 min at 12 000 g and 4°C. The RNA-containing fraction was mixed with 250 μl isopropanol and incubated for 10 min.

Next, the samples were centrifuged at 10 000 g and 4°C for 10 min and the RNA pellets resuspended in 75% ethanol. After centrifugation for 5 min at 7500 g and 4°C, the RNA pellets were air-dried and the RNA dissolved in nuclease-free water. The RNA concentration was measured using a NanoDrop™ One UV/Vis spectrophotometer (Thermo Fisher Scientific).

2.9.2 | Reverse transcription and quantitative real-time PCR (RT-qPCR)

To transcribe the purified RNA into single-stranded cDNA, the First Strand cDNA synthesis kit (Thermo Fisher Scientific) was used according to the manufacturer's protocol. Briefly, a reaction mix containing 1 µl RNase inhibitor, 2 µl dNTP mix, 2 µl reverse transcriptase, 1 µl Oligo(dT)₁₈ primers and 4 µl 5× reaction buffer was prepared and mixed with 1 µg of isolated RNA. The reverse transcription was performed in a Biometra thermocycler (Analytik Jena AG, Jena, Germany) with following incubation settings: 1 h at 37°C, 5 min at 70°C, cooling down to 4°C. RT-qPCR was performed using ORA™ SEE qPCR Green ROX H Mix (HighQu, Kraichtal, Germany) and specific mouse primer pairs (Eurofins, Ebersberg, Germany). The following primers were used: *MIF* forward: ACA GCA TCG GCA AGA TCG and *MIF* reverse: AGG CCA CAC AGC AGC TTA C; *Il-1β* forward: GAA ATG CCA CCT TTT GAC AGT G and *Il-1β* reverse: TGG ATG CTC TCA TCA GGA CAG; *Ifn-γ* forward: CAG CAA CAG CAA GGC GAA AAA GG and *Ifn-γ* reverse: TTT CCG CTT CCT GAG GCT GGA T; *Il-6* forward: ATG GAT GCT ACC AAA CTG GAT and *Il-6* reverse: TGA AGG ACT CTG GCT TTG TCT; *Cxcl1* (*Kc*) forward: TCC AGA GCT TGA AGG TGT TG and *Cxcl1* (*Kc*) reverse: AAC CAA GGG AGC TTC AGG GT; *Cd3* forward: TCA GCC TCC TAG CTG TTG G and *Cd3* reverse: GTC AAC TCT ACA CTG GTT CC; *FoxP3* forward: TTC ATG CAT CAG CTC TCC AC and *FoxP3* reverse: CTG GAC ACC CAT TCC AGA CT; *actin* forward: GGA GGG GGT TGA GGT GTT and *actin* reverse: GTG TGC ACT TTT ATT GGT CTC AA. PCR reactions were run in a Rotorgene Q (Qiagen). Relative mRNA levels were calculated using the $\Delta\Delta C_t$ method with *actin* as a house-keeping gene.

2.10 | Lipid analysis

2.10.1 | Cholesterol fluorometric assay

Cholesterol levels in plasma were measured using Cayman's Cholesterol Fluorometric Assay Kit (Cayman

Chemicals/Biomol GmbH, Hamburg, Germany) according to the manufacturer's instructions. Briefly, plasma was diluted 1:2000 in cholesterol assay buffer and 50 µl of the samples were added to the wells of a 96-well plate. After initiation the reaction with 50 µl of assay cocktail (4.745 ml cholesterol assay buffer, 150 µl cholesterol detector, 50 µl cholesterol assay HRP and 5 µl cholesterol esterase), the plates were incubated for 30 min at 37°C in the dark. Afterward, the fluorescence was measured at an excitation wavelength of 535 nm and an emission wavelength of 590 nm. Samples were measured in duplicates using an EnSpire Multimode Plate Reader (PerkinElmer). Diluted cholesterol standards with final concentrations between 2 and 20 µM were used for the quantification of cholesterol levels in the plasma.

2.10.2 | Triglyceride colorimetric assay

Triglyceride levels in plasma were measured using Cayman's Triglyceride Colorimetric Assay Kit (Cayman Chemicals/ Biomol GmbH) according to the manufacturer's instruction. Briefly, 10 µl of undiluted plasma was mixed with 100 µl of prediluted enzyme mixture in a 96-well plate and incubated for 15 min at RT. The absorbance was measured at 540 nm using the EnSpire Multimode Plate Reader (PerkinElmer). Diluted triglyceride standards with final concentrations between 3.125 and 200 mg/dl were used for the quantification of triglyceride levels in mouse plasma.

2.11 | Murine MIF ELISA

MIF levels in murine plasma were measured by the Mouse MIF DuoSet® ELISA (R&D Systems) according to the manufacturer's instruction. Briefly, wells of a 96-well plate were coated with 100 µl of capture antibody at a final concentration of 400 ng/ml overnight at RT. After three washes with washing buffer (0.05% Tween 20 in PBS, pH 7.2), plates were blocked in 300 ml of 1× reagent diluent concentrate 2 (R&D Systems) for 1 h at RT. After additional washing, 100 µl of the appropriately diluted plasma sample or standard in 1× reagent diluent concentrate 2 was added into each well. Standards were prepared using the recombinant mouse MIF standard supplied with the kit using twofold serial dilutions. Standard concentrations ranged from 125 to 2000 pg/ml. After incubation with samples/standards for 2 h at RT, washing was repeated as described, and 100 µl of detection antibody at a final concentration of 200 ng/ml were added for 2 h at RT. Plates were washed three times, 100 µl of Streptavidin-HRP (1:200 dilution) added, and

incubated for 20 min at RT, followed by washing and incubation with 100 μ l of TMB substrate solution (Thermo Fisher Scientific) for another 20 min at RT. The reaction was stopped by adding 50 μ l of stop solution (2N H₂SO₄) per well. Optical density was determined at 450 nm using an EnSpire Multimode Plate Reader (PerkinElmer). Plasma dilutions of 1:50 and 1:100 were found to be optimal for best signal/noise ratios, and mean values were used for analysis.

2.12 | Multiplex cytokine and chemokine quantification by Luminex

Plasma concentrations of cytokines and chemokines: ENA-78 (CXCL5), eotaxin (CCL11), G-CSF (CSF-3), GM-CSF, GRO- α (CXCL1), IFN- α , IFN- γ , IL-1 α , IL-1 β , IL-10, IL-12p70, IL-13, IL-15, IL-17A (CTLA-8), IL-18, IL-2, IL-22, IL-23, IL-27, IL-28, IL-3, IL-31, IL-4, IL-5, IL-6, IL-9, IP-10 (CXCL10), LIF, M-CSF, MCP-1 (CCL2), MCP-3 (CCL7), MIP-1 α (CCL3), MIP-1 β (CCL4), MIP-2 α (CXCL2), RANTES (CCL5), and TNF- α were measured using a multiplex x-MAP magnetic bead-based immunoassay kit (ProcartaPlex Mouse Cytokine and Chemokine Convenience panel 1A 36-Plex, #EPXR360-26092-901, Invitrogen (Karlsruhe, Germany)). The assay was performed according to the manufacturer's instructions. Frozen plasma from mice of the 24- and 42-week HFD groups was thawed, homogenized, and centrifuged at 17000 rpm for 5 min to remove debris and excess lipid droplets. Samples and manufacturer-supplied cytokine standards (standard mix A #287083-000 and mix 1B #288534-00) were diluted 1:6 and 1:4, respectively, in 1 \times universal assay buffer (UAB) and run as duplicates in 96-well flat-bottom plates. Analysis was performed on a Luminex 200 system using xPONENT v. 3.1 software (Luminex Corporation, Austin, USA). Washing steps were conducted using a hand-held magnetic plate washer (Invitrogen). The doublet discrimination (DD) gate was set at 7500–25000, the sample volume was 50 μ l, and at least 50 events per bead were recorded. The concentration of the different analytes was calculated using ProcartaPlex Analysis App software (Invitrogen). Concentrations under the detection limit were defined as 0. Data analysis and standard curve fitting were performed using a five-parameter logistic (5PL) fitting model.

2.13 | Smart seq2-based RNA sequencing from brachiocephalic artery (BCA) sections

Five micrometer OCT-embedded frozen sections from the BCA were gently thawed (room temperature, 5 min).

Sections were immersed in 50 μ l of freshly prepared RNA isolation buffer 20% proteinase K (Qiagen, Hilden, Germany) and 1:2400000 ERCC RNA spike-in mix in buffer PKD (Thermo Fisher Scientific) for approximately 30 s to permit lysis and homogenization of the whole BCA tissue. A 200- μ l tip was used to scratch the BCA tissue lysate from the glass slide under a microscope. The BCA lysates from 3 to 4 BCA sections were pooled and collected in a 1.5 ml reaction tube and frozen at -80° C. The RNA in the BCA lysates was purified and washed with oligo dT25 magnetic beads (Thermo Fisher Scientific), followed by removing the beads via incubating the samples at 80° C and placing the samples on a magnet. For library construction, 1 ng RNA was taken from each sample for reverse transcription and cDNA amplification following a Smart-seq2 protocol, followed by library construction as described before.^{34,35} Briefly, samples were first thawed and then incubated for 3 min at 72° C and immediately placed on ice followed by the steps of reverse transcription (RT) and pre-amplification. The cDNA was then cleaned using AMPure bead (Beckman-Coulter) clean-up at a 0.7:1 beads:PCR product ratio. Libraries were assessed using Bio-analyzer (Agilent, catalog no. 2100), and the High Sensitivity DNA analysis kit, and also fluorometrically using Qubit's DNA HS assay kits and a Qubit 4.0 Fluorometer (Invitrogen, Life Technologies) to measure the cDNA concentrations. After normalization to 160 pg/ μ L, 1.25 μ l of cDNA samples were used for library construction using in-house Tn5 transposase. Libraries were barcoded and pooled, then cleaned up with three rounds of AMPure bead (Beckman-Coulter) at a 0.8:1 ratio beads:library. Libraries were sequenced 2 \times 100 reads bp paired-end on a DNB-seq platform to an average depth of 3 \times 10⁶ reads per sample. Sequencing was performed by BGI Tech Solutions Co., Limited (Hongkong, China).

2.14 | RNA-Seq data processing and analysis

Following trimming with Trim Galore (<https://github.com/FelixKrueger/TrimGalore>, <https://doi.org/10.14806/ej.17.1.200>) and quality control with FastQC (<https://www.bioinformatics.babraham.ac.uk/projects/fastqc/>), STAR³⁶ was used to align the reads to the GRCm39 mouse genome. "quantMode GeneCounts" argument of STAR was used during alignment and unstranded counts were collected. For filtering low-count genes, genes that have <20 reads and are expressed by <4 samples were filtered, resulting in 9578 genes. Subsequently, DESeq2 was utilized to analyze the differential expression genes between groups. Data shown in boxplot and heatmap were normalized with the

blinded variance-stabilizing transformation from the vsn Bioconductor package.³⁷

2.15 | Statistics

All statistical analyses were performed using GraphPad Prism 6.0 or 7.0 (GraphPad Software Inc.). Data are represented as means \pm SD. After testing for normality using the *D'Agostino*–Pearson test, data were analyzed by two-tailed Student's *t*-test (parametric) or by Mann–Whitney test (non-parametric) as appropriate. In case of comparing more than two groups, two-way ANOVA with Sidak's multiple comparisons test was applied. Bulk RNA-Seq differential expression analyses were performed with Wald test from the DESeq2 package.³⁸ $p < .05$ was considered statistically significant.

3 | RESULTS

3.1 | Atheroprotection due to global *Mif* deficiency in *Apoe*^{-/-} mice is reduced upon aging

The role of MIF in atherogenesis has previously been investigated in younger and middle-aged atherogenic *Apoe*^{-/-} or *Ldlr*^{-/-} mice on HFD for up to 14–26 weeks.^{18,20–23,39} However, age-dependent effects of MIF were not addressed in these studies. Here, we determined the effect of global *Mif* deficiency in 30-, 42-, and 48-week-old *Apoe*^{-/-} mice that received an HFD for 24, 36, and 42 weeks, respectively, as well as in 52-week-old mice that received an HFD in the last 6 weeks, that is, in 30/24-, 42/36-, 48/42-, and 52/6-week treatment groups.

We first compared the body weights of *Apoe*^{-/-}*Mif*^{-/-} mice with those of *Apoe*^{-/-} controls over the course of aging and HFD. As expected, the body weight of *Apoe*^{-/-} control mice increased with age and the duration of the HFD (24 weeks HFD: 35.4 \pm 4.8 g; 42 weeks HFD: 38.2 \pm 5.5 g). The same was observed for the respective *Mif*-deficient animals (24 weeks HFD: 34.0 \pm 3.7 g; 42 weeks HFD: 32.6 \pm 3.3 g). The observed apparent reduced weight gain in the *Mif*-deficient mice did not reach statistical significance (Table S1). We next determined the lipid levels in these age/treatment groups. We detected significantly decreased triglyceride levels in the plasma of *Apoe*^{-/-}*Mif*^{-/-} mice after 42 weeks of HFD diet compared to *Apoe*^{-/-} controls (Table S2; *Apoe*^{-/-}*Mif*^{-/-}: 116.9 \pm 28.9 g; *Apoe*^{-/-}: 211.4 \pm 88.2 g; $p = .025$). By contrast, cholesterol levels in the *Apoe*^{-/-}*Mif*^{-/-} mice both after 24 and 42 weeks of HFD did not significantly differ from those in *Apoe*^{-/-} controls (Table S2). Furthermore,

adiponectin and leptin mRNA expression levels did not differ between *Apoe*^{-/-} and *Apoe*^{-/-}*Mif*^{-/-} mice, when compared in the 30/24-week group (Figure S1). Also, additional blood parameters such as total white blood cell count (WBC), red blood cells (RBC), hemoglobin (HGB), and hematocrit (HCT) did not differ between mouse strains and age groups (Table S3). In summary, with the exception of triglyceride levels, blood parameters, lipids, and body weight did not MIF-dependently differ across aging and duration of HFD.

We next analyzed the atherosclerotic lesions across the vascular tree. Plaque area analysis in the 30/24-week group confirmed the atheroprotective effect of *Mif*-gene deletion that had been previously observed in atherogenic mice with an *Apoe*^{-/-} background, and also confirmed the previously noted regio-dependent restriction.²³ To this end, *Apoe*^{-/-}*Mif*^{-/-} mice exhibited a significantly reduced plaque size compared with *Apoe*^{-/-} controls in BCA and abdominal aorta, but not in aortic root, aortic arch, and thoracic aorta (Figure 1). Notably, the atheroprotective effect of *Mif*-knockout was lost over the time course of aging and HFD. While attenuation of plaque formation in the *Mif*-knockout genotype was still observed in the BCA and abdominal aorta after 36 weeks of HFD, it was lost in the 48/42-week group (Figure 1A,B,E,F,I), with an almost inverted plaque phenotype seen in abdominal aorta of the most aged animals of 48/42 weeks (Figure 1I). The loss of the atheroprotective phenotype in *Mif*-deficient mice at an advanced age of 48 weeks was further confirmed in the 52/6-week mouse group. No difference in plaque size was seen in those mice, neither in aortic root, arch, and thoracic aorta, nor in BCA and abdominal aorta (Figure S2A–H). An observed decrease in aortic root plaque area in the *Mif*-deficient mice 48/42-week group (but not the 30/24 group) is interesting, but differs from all other effects seen in this advanced age/HFD group, and would need future exploration. The similar outcome in the 48/42- and 52/6-week models could be indicative of an increasing dominant effect of aging per se over the duration of the HFD in an atherogenic *Apoe*^{-/-} background.

MIF expression levels may decrease over the course of aging,⁴⁰ and this may lead to a relative reduction in the difference in MIF levels between *Apoe*^{-/-}*Mif*^{-/-} and *Apoe*^{-/-} mice, in turn affecting the differences seen in atheroprotection upon *Mif* deficiency at different age stages. However, quantification of MIF expression levels in liver and spleen by qPCR as well as plasma MIF determinations by ELISA did not reveal differences in MIF levels in *Apoe*^{-/-} mice after 24 versus 42 weeks of HFD, that is, in 30- versus 48-week-old mice (Figure S3).

The comparison of plaque phenotypes across age, HFD duration, and vascular bed locations led to additional interesting observations irrespective of the investigation of

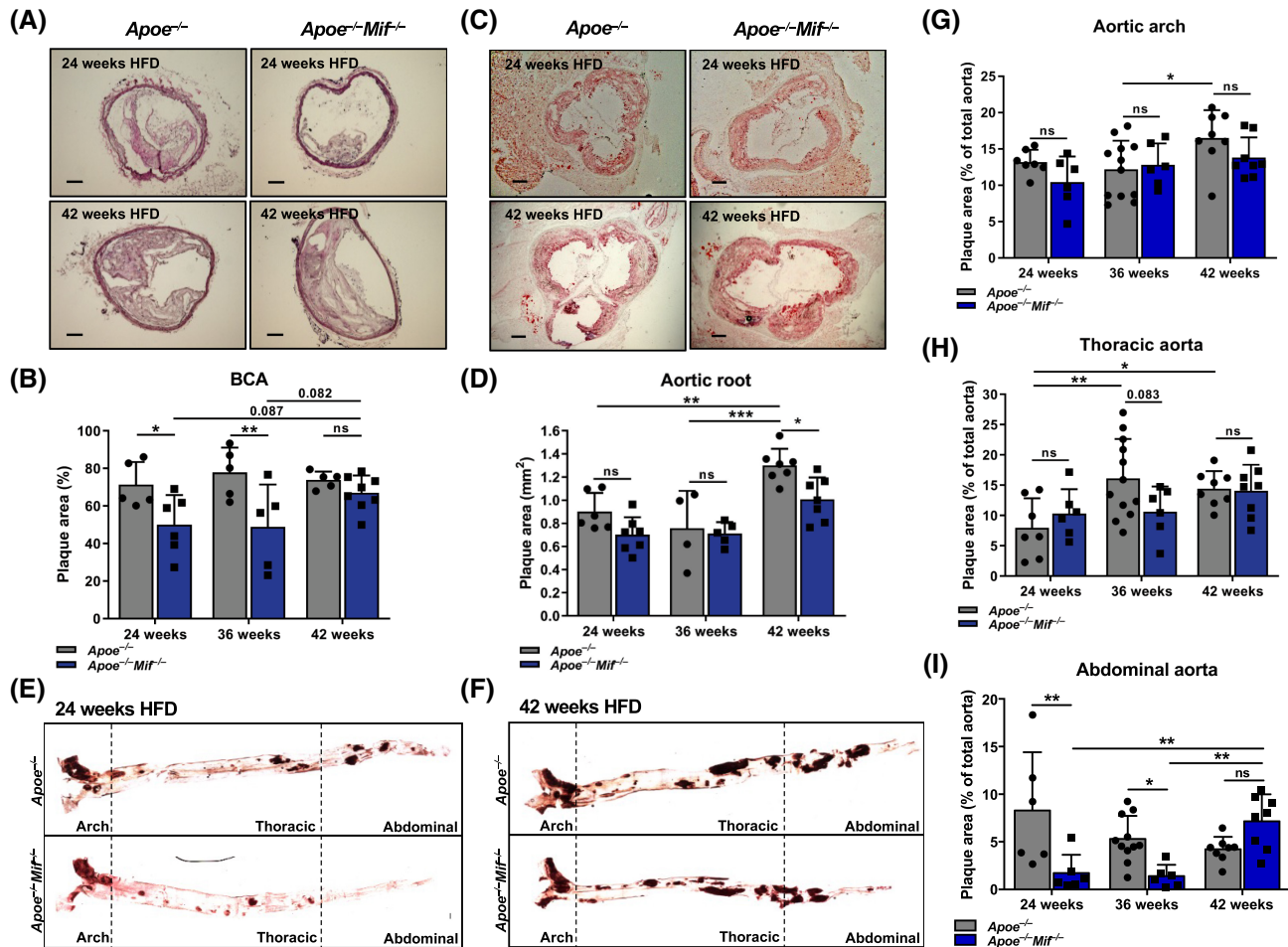


FIGURE 1 Atheroprotection due to *Mif* deficiency is attenuated in highly aged hyperlipidemic *Apoe*^{-/-} mice. Atherosclerotic plaques were quantified in BCA, aortic root, aortic arch, thoracic, and abdominal aorta of 30-, 42-, and 48-week-old *Apoe*^{-/-}*Mif*^{-/-} mice after 24, 36, and 42 weeks of HFD, respectively, (blue) and compared with corresponding lesions in *Apoe*^{-/-} mice (gray). (A,B) Representative images (A) and plaque quantification (B) of H&E-stained BCA sections. For each mouse, 12 serial sections with a distance of 50 μ m were used for analysis. The mean plaque area is depicted as percentage of the total inner vessel area including the plaque ($n = 5-8$ mice, results are presented as means \pm SD; scale: 100 μ m). (C,D) Representative images (C) and quantification (D) of ORO-stained sections of the aortic root. Serial sections were obtained as in (A,B). The mean plaque area is depicted in mm² ($n = 4-7$ mice, results are shown as means \pm SD; scale: 200 μ m). (E,F) Representative images of *en face*-prepared and ORO-stained aortas after 24 (E) and 42 (F) weeks of HFD. (G-I) Quantification of plaque area in aorta including aortic arch (G), thoracic aorta (H), and abdominal aorta (I). The plaque area is depicted as percentage of the total aortic surface ($n = 6-12$ mice, results presented as means \pm SD). Statistics: two-way ANOVA with Sidak's multiple comparisons test. * $p < .05$; ** $p < .01$; ns, nonsignificant; nonsignificant results with p -values between .05 and .1 are given as precise numbers; each data point represents one independent mouse).

Mif deficiency. In the BCA of *Apoe*^{-/-} mice, plaque burden stagnated at approximately 75% plaque area after 24 weeks of HFD (Figure 1B), whereas an aging/HFD duration-dependent increase was observed in aortic root, arch, and thoracic aorta (Figure 1D,G,H). A trend toward a decrease in plaque burden was noted in the abdominal part of the aorta (Figure 1I).

In conclusion, atherosclerotic lesion analysis confirmed that *Mif* deficiency in *Apoe*^{-/-} mice attenuates lesion formation but also showed that the atheroprotective effect of global *Mif* deletion in BCA and abdominal aorta is reduced or lost at a highly advanced age. Thus,

aging seems to be a contributing factor, when considering MIF-mediated effects during atherosclerotic disease progression.

3.2 | CD4⁺ T-cell numbers in spleen and blood are changed in an age- and MIF-dependent manner

To begin to explore the mechanisms underlying the observed age- and MIF-dependent plaque phenotype, we applied flow cytometry to analyze immune cell populations

in spleen, blood, LNs, and BM. Cell numbers were compared for the 24- and 42-week HFD treatment regimens between *Apoe*^{-/-} and *Apoe*^{-/-}*Mif*^{-/-} mice. Interestingly, the most significant changes were seen for T cells.

Total splenic T-cell levels were significantly reduced in *Apoe*^{-/-} mice over the course of aging, and a subpopulation analysis showed that this effect was due to a decrease in CD4⁺ T cells, whereas CD8⁺ T-cell numbers remained unchanged (Figure 2A). A similar effect was observed for circulating T cells, although differences did not reach

statistical significance, while no changes were noted for T cells isolated from LNs or BM (Figure 2B–D). The T-cell analysis also revealed a significant influence of MIF. Splenic CD4⁺ T-cell numbers in *Apoe*^{-/-}*Mif*^{-/-} mice were significantly increased compared with T-cell numbers in spleens from *Apoe*^{-/-} mice, both at 24 and 42 weeks of HFD, with a more pronounced difference seen at 42 weeks (Figure 2A). This effect in the aged 48/42-week mice was further confirmed in the 52/6-week aging/HFD model (Figure S2I). While no MIF-dependent changes were

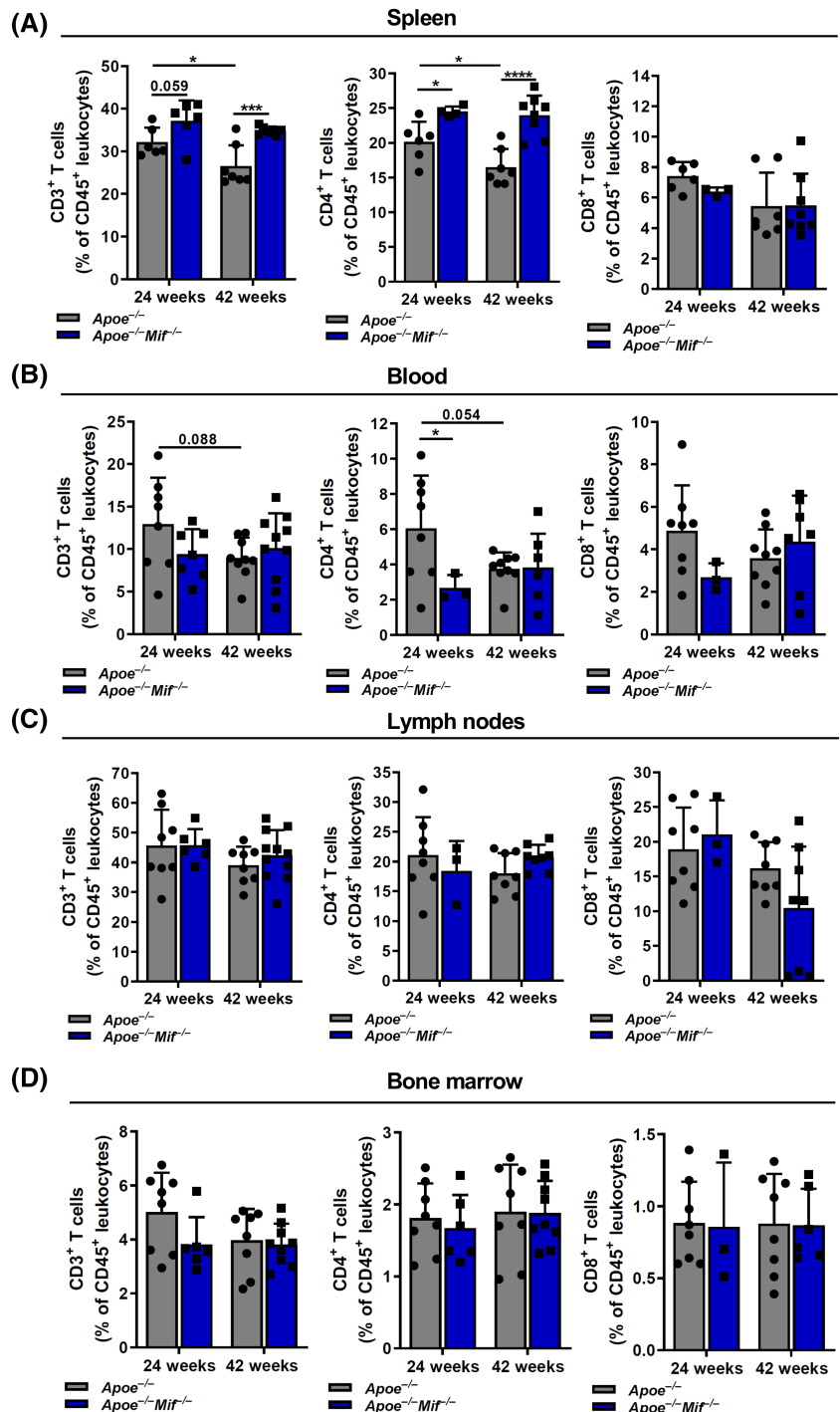


FIGURE 2 CD4⁺ T-cell numbers in spleen and blood of hyperlipidemic *ApoE*^{-/-} mice change in a MIF and age-dependent manner. FACS-based quantification of total CD3⁺ T cells (left panels), CD4⁺ T-cell subsets (middle panels), and CD8⁺ T-cell subsets (right panels) in spleen (A), blood (B), lymph nodes (C), and bone marrow (D) of *ApoE*^{-/-}*Mif*^{-/-} mice (blue) and comparison to *ApoE*^{-/-} controls (gray). 30- and 48-week-old mice on HFD for 24 and 42 weeks, respectively, were examined. Bars shown represent data from *n* = 3–8 independent mice and results are shown as means ± SD. Statistics: two-way ANOVA with Sidak's multiple comparisons test. **p* < .05, ****p* < .001; *****p* < .0001, nonsignificant results with *p* values between .05 and .1 are indicated.

observed for T cells from LN or BM (Figure 2C,D), blood CD4⁺ T-cell numbers were lower in *Apoe*^{-/-}*Mif*^{-/-} mice compared with *Mif*-expressing controls in the 30/24- as well as in the 52/6-week group (Figure 2B, Figure S2J).

We also determined B-cell, monocyte, and neutrophil counts in spleen, LN, BM, and blood. While monocyte counts were not altered between age groups or as a function of MIF, some changes were seen for B cells and neutrophils such as a decrease in LN B cells in 24-week HFD-fed *Apoe*^{-/-}*Mif*^{-/-} mice, an increase in CD19⁺ B cells in the blood and in the LNs of *Apoe*^{-/-}*Mif*^{-/-} mice at 42 weeks HFD, while splenic B cells were decreased at 42 weeks HFD. BM neutrophils were increased in 24-week HFD-fed *Apoe*^{-/-}*Mif*^{-/-} mice and decreased between the 24- and 42-week *Mif*-deficient groups (Figure S4). Overall, these changes did not give rise to an apparent consistent pattern that could readily explain the observed plaque phenotype. Together, the immune cell analysis in blood and peripheral lymphoid organs indicated that especially CD4⁺ T-cell numbers in the spleen and blood may be controlled in a MIF- and age-dependent manner.

3.3 | The enhancement of lesional Trem2⁺ macrophage and T-cell counts in *Mif*-deficient *Apoe*^{-/-} mice is lost over the course of aging

To further investigate the unraveled plaque phenotype, we analyzed SMCs, macrophages, and T cells in plaques of the BCA after 24 and 42 weeks of HFD. The content of smooth muscle actin (SMA)⁺ SMCs was unaltered upon *Mif* deficiency and aging (Figure 3A,B). By contrast, we detected substantial changes in plaque macrophage numbers (Figure 3C,D).

As indicated by vessel staining with an anti-CD68 antibody, macrophage numbers in plaques of *Apoe*^{-/-}*Mif*^{-/-} mice fed an HFD for 24 weeks were significantly increased compared with those in *Apoe*^{-/-} mice; intriguingly, this increase was gone in the 42-week HFD regimen. This was mainly due to a significant decrease in macrophages numbers in the *Apoe*^{-/-}*Mif*^{-/-} mice over the course of aging (Figure 3C,D). We hypothesized that the aging stage-dependent difference in macrophage count in the *Apoe*^{-/-}*Mif*^{-/-} mice could involve macrophage subsets with an anti-inflammatory or atheroprotective phenotype. One subset is lipid-loaded “foamy” Trem2^{hi} macrophages. Single-cell (sc) RNA-Seq analysis revealed an accumulation of these cells within atherosclerotic lesions and showed that they display an anti-inflammatory and homeostatic transcriptional signature.⁴¹⁻⁴³ Following verification of the specificity of the commercially available anti-Trem2 antibody (Figure S5), which also had been

previously used to stain Trem2⁺ microglia in brain,³³ we analyzed our plaque specimens for Trem2⁺ macrophages and found that Trem2⁺ cells in plaque areas of *Mif*-deficient *Apoe*^{-/-} mice were significantly reduced after 42 weeks of HFD, when compared to the respective 24-week HFD group, whereas no age/HFD-dependent difference in lesional Trem2⁺ cells was seen in the *Apoe*^{-/-} control group (Figure 3E,F; Figure S6). The determination of Trem2⁺ Ki67⁺ cells indicated that the observed alteration in lesional Trem2⁺ cells could be due to an effect of MIF on the proliferative capacity of these cells. To this end, Trem2⁺ Ki67⁺ cells were increased in the 24-week *Mif*-deficient *Apoe*^{-/-} mice compared with *Apoe*^{-/-} mice, while they were decreased in the *Mif*-deficient *Apoe*^{-/-} mice after 42 weeks of HFD compared with the *Mif*-deficient 24-week group (Figure 3G,H; Figure S6). A link between MIF and the proliferative capacity of Trem2⁺ macrophages was further supported by experiments with bone marrow-derived macrophages (BMDMs). The proliferative capacity of these cells was assessed by flow cytometry following incorporation of Edu. BMDMs isolated from *Apoe*^{-/-} mice had a higher proliferative capacity in the 42-week HFD group compared with cells from mice on HFD for 24 weeks. Of note, the number of Trem2⁺ Edu⁺ BMDMs isolated from the 42-week HFD *Apoe*^{-/-} mouse group was halved in the 42-week HFD *Apoe*^{-/-}*Mif*^{-/-} BMDM group (Figure S7). Together, this indicated that *Mif* deficiency facilitates the proliferation of Trem2⁺ macrophages and that this effect is attenuated in mice of a more advanced age.

Given the detected apparent influence of MIF and aging on peripheral T-cell numbers, we next quantitated lesional T cells. CD3⁺ T-cell numbers were significantly elevated in *Mif*-deficient *Apoe*^{-/-} mice after 24 weeks of HFD compared with the *Apoe*^{-/-} control group. By contrast, no difference was observed between the genotypes after 42 weeks of HFD and CD3⁺ T-cell numbers were significantly downregulated in the 42-week HFD *Apoe*^{-/-}*Mif*^{-/-} group compared with 24-week HFD-fed *Apoe*^{-/-}*Mif*^{-/-} mice (Figure 3I,J). The upregulation of T cells in *Mif*-deficient *Apoe*^{-/-} mice after 24 weeks of HFD was confirmed by RT-qPCR measurements for CD3 from plaque tissue (Figure S8). In following up on the hypothesis that the elevated T-cell population could represent—at least in part—regulatory T cells (Tregs), which are considered anti-atherogenic, we performed immunofluorescent staining and qPCR for lesional Tregs, but, due to the very low number of such cells in the vascular wall, were unable to obtain quantifiable results for this cell type. Moreover, a quantification of FoxP3 mRNA expression levels from spleen as an indicator of Tregs showed that the abundance of splenic FoxP3⁺ cells did not differ between 24-week HFD-fed *Apoe*^{-/-} and *Apoe*^{-/-}*Mif*^{-/-} mice. By contrast,

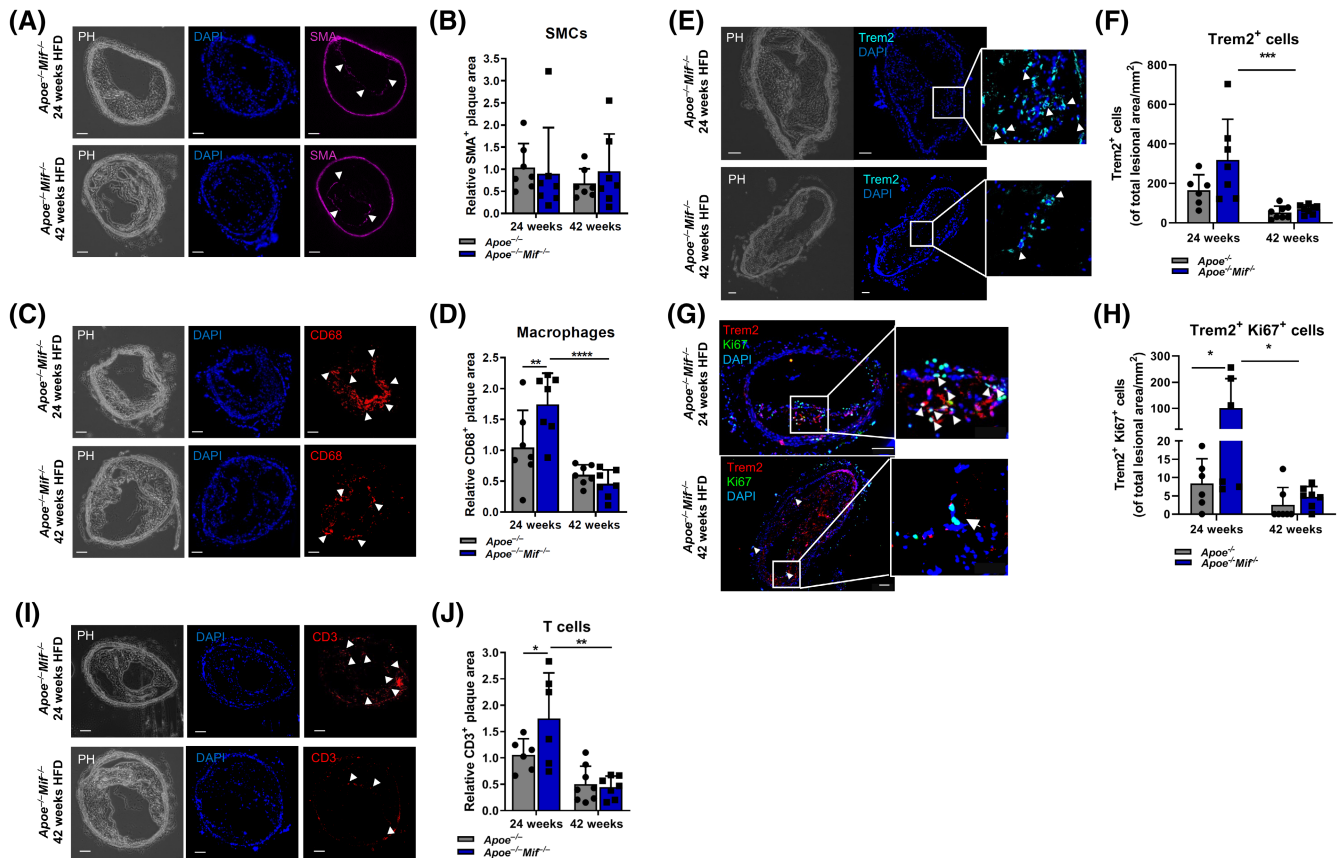


FIGURE 3 Age- and MIF-dependent changes in lesional total macrophage and Trem2⁺ macrophage numbers. Immunohistochemistry was performed on BCA sections derived from 30- and 48-week-old *Apoe^{-/-}Mif^{-/-}* (blue) and *Apoe^{-/-}* (gray) mice after 24 and 42 weeks of HFD, respectively. Smooth muscle cells (SMA), total macrophage content (CD68), and Trem2⁺ macrophages were quantified in the plaque area. Nuclear counterstain was performed using DAPI. (A,B) Representative images (A) and quantification (B) of the SMA⁺ plaque area. Two to three sections were analyzed per mouse, and mean values normalized to values of the 30-week-old *Apoe^{-/-}* controls that received HFD for 24 weeks (*n* = 7 mice; results presented as means ± SD; scale bar: 100 μm; arrows indicate the SMA⁺ plaque area; PH = phase contrast). (C,D) Representative images (C) and quantification (D) of the CD68⁺ plaque area. Analysis performed as in (A,B) (*n* = 7 mice, results are presented as means ± SD; scale bar: 100 μm; arrowheads indicate the CD68⁺ plaque area). (E,F) Representative images (E) and quantification (F) of Trem2⁺ cells within the plaque. Cells are indicated by arrowheads in the enlarged image sections. Trem2⁺ cells were quantified manually and are depicted as Trem2⁺ cells per mm² plaque area. As Trem2 is mainly expressed by myeloid cells, the stained cells were considered as Trem2⁺ macrophages. G-H) Representative images (G) and quantification (H) of lesional Trem2⁺ Ki67⁺ cells. Trem2⁺ Ki67⁺ cells are indicated by arrowheads in the enlarged image sections. Trem2⁺ Ki67⁺ double-positive cells were manually quantified and are depicted as Trem2⁺ Ki67⁺ cells per mm² plaque area. (I,J) Representative images (I) and quantification (J) of lesional CD3⁺ T cells. Arrowheads indicate the CD3⁺ plaque area. Results are presented as means ± SD from *n* = 6–8 mice; scale bar: 100 μm. Statistics: two-way ANOVA with Sidak's multiple comparisons test. **p* < .05; ***p* < .01; ****p* < .001; *****p* < .0001; each data point represents one independent mouse.

splenic FoxP3⁺ cells were elevated in *Apoe^{-/-}Mif^{-/-}* mice after 42 weeks of HFD but not in the 24-week HFD group (Figure S8). Overall, this is a hint that T-cell subtypes other than Tregs may be linked to the observed plaque phenotype in *Mif*-deficient mice upon aging. Together, the analysis of lesional immune cells in the BCA suggests that atheroprotection in 24-week HFD-fed *Apoe^{-/-}Mif^{-/-}* mice and the attenuation of atheroprotection in these mice across the course of advanced aging is associated with an increase and subsequent reduction in lesional Trem2⁺ macrophages and T cells.

3.4 | Transcriptomics identifies MIF- and aging-dependent pathways and key enriched genes

To get further insight into the cellular and molecular parameters associated with the observed MIF- and age-dependent plaque phenotype, we analyzed the transcriptome of BCA plaque tissue from *Apoe^{-/-}* and *Apoe^{-/-}Mif^{-/-}* mice, both after 24 and 42 weeks of HFD. Plaques from four mice were analyzed in each group. RNA was isolated from the BCA sections and smart seq2-based

bulk RNA sequencing performed following a previously established procedure.³⁵ Following quality control of the obtained libraries, 9578 genes passed the low-count filtering and were used for comparison between the four groups and pathway enrichment analysis.

Transcriptomic analysis as shown by Volcano plot and gene ontology (GO) identified various significant changes (Figure 4, Figure S9, Tables S4–S6). When comparing the *ApoE*^{-/-} and *ApoE*^{-/-}*Mif*^{-/-} genotypes upon 24-week HFD, out of 154 genes, which are significantly differentially expressed between these genotypes after 24 weeks of HFD (Table S4), several genes, related to the “lipid biosynthesis and metabolism” and “brown adipose cell differentiation” pathways, were enriched in the *ApoE*^{-/-} genotype (Figure 4A,B,E). Most highly and significantly enriched were genes such as *Plin1* and *Plin4* (lipid storage) (Figure 4A,E,F), genes that encode for the lipid droplet-associated proteins perilipin 1 and perilipin 4, respectively, and have been associated with foam cells^{44,45};

Tnnt3 (troponin T3, muscle contraction) (Figure 4A,F), a gene best known for its expression in fast skeletal type muscles, but which has also been identified by microarray screening to be upregulated in aorta from *ApoE*^{-/-} mice upon HFD and statin cotreatment⁴⁶; *Thrsp* (regulation of lipid synthesis) (Figure 4A,F), the gene encoding for thyroid hormone-responsive spot 14, suggested to be a master regulator of lipogenesis and implicated in nonalcoholic steatohepatitis (NASH)^{47,48}; and *Ldlr* (lipid transport and metabolism) (Figure 4A,F), the gene encoding for the LDL receptor and one of the top atherosclerosis-related genes due to its key role in reducing plasma LDL-cholesterol, but also contributing to plaque foam cell formation.^{49,50} The most pronounced enriched pathways in the *ApoE*^{-/-}*Mif*^{-/-} group were “ATP activity and muscle contraction” (Figure 4A,B), but also “regulation of myeloid leukocyte-mediated immunity.” Strongly enriched genes comprised *Rnd1*, *Jaml*, and *Col4a4* (Figure 4A,E), encoding for the small Rho family GTPase Rnd1, junctional

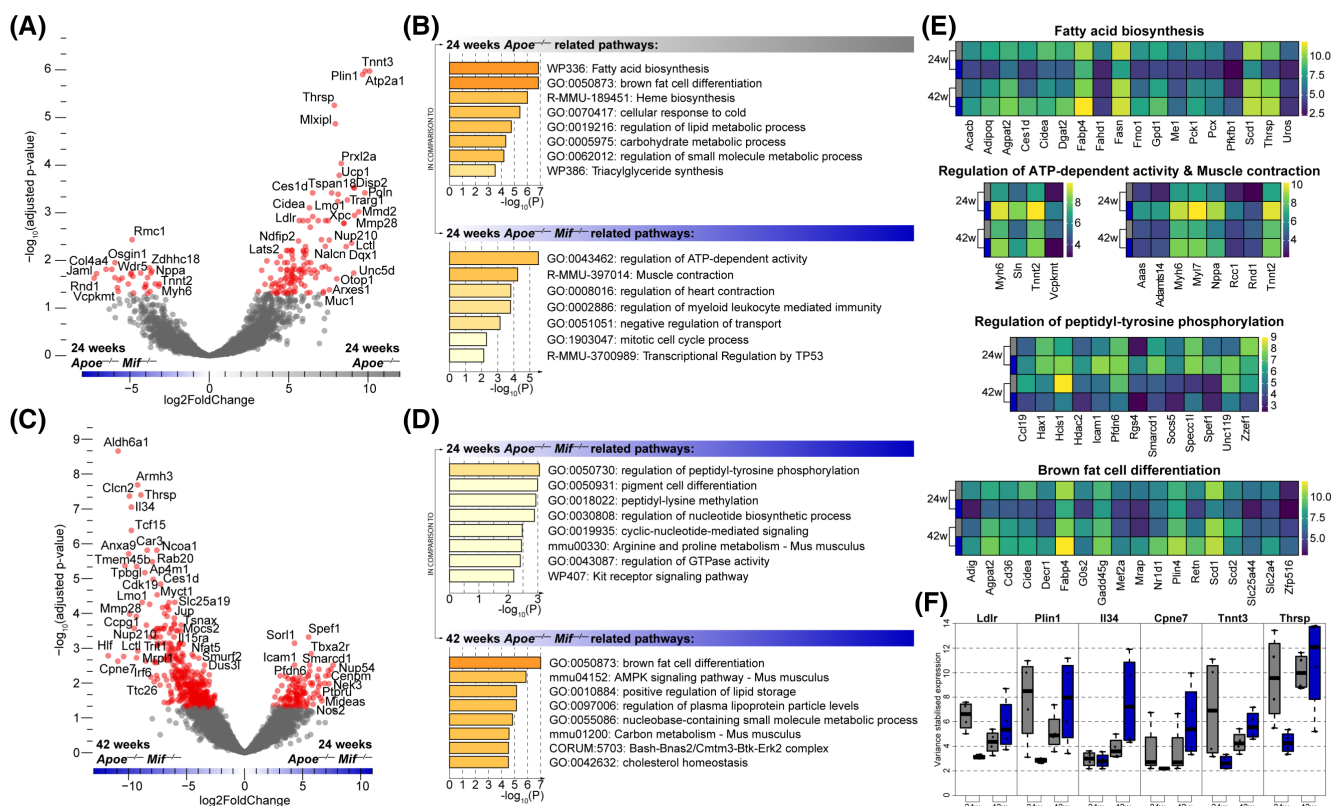


FIGURE 4 MIF- and age-dependent changes in the transcriptomic signature of atherosclerotic lesions. Differential expression analysis was performed on bulk RNA-Seq data of BCA tissue sections from *ApoE*^{-/-} and *ApoE*^{-/-}*Mif*^{-/-} mice on a 24- and 42-week hyperlipidemic diet (HFD). (A,B) Volcano plot (A) and top-enriched pathways (B) of the differential gene expression (DGE), comparing the *ApoE*^{-/-} and *ApoE*^{-/-}*Mif*^{-/-} genotypes upon 24-week HFD. (C,D) Volcano plot (C) and top-enriched pathways (D) of the DGE, comparing the 24- to the 42-week HFD differences within the *ApoE*^{-/-}*Mif*^{-/-} genotype. (E) Heatmaps of the top 5 pathways from the comparisons presented in (A,B) and (C,D). For each pathway, a maximum of 18 significant genes are depicted for space constraints (full lists in Tables S4 and S5). Expression values are the variance-stabilized expression values (see Methods). (F) Boxplot of expression of main genes mentioned in the Results section. Transcriptomic analysis was performed on *n* = 4 mice per group. Each dot shown is an independent mouse/sample. Expression values are the variance-stabilized expression values (see Methods). Grey bars, *ApoE*^{-/-}; blue bars, *ApoE*^{-/-}*Mif*^{-/-}.

adhesion molecule-like, a JAM family adhesion molecule involved in leukocyte trafficking, and the type IV collagen Col4A4,⁵¹ respectively.

Overall, more genes but less pronounced and less significant differences were observed, when comparing the *Apoe*^{-/-} and *Apoe*^{-/-}*Mif*^{-/-} genotypes after 42 weeks of HFD (Figure S9 and Table S6). Eight hundred fifty-four genes were found to be differentially expressed between these groups. The most upregulated pathways in the *Apoe*^{-/-} genotype were related to “glomerular filtration” and “nucleus and chromatin organization,” as well as “cell death,” while pathways related to “VEGF, PI3K, and MAPK signaling” were most strongly enriched in the *Apoe*^{-/-}*Mif*^{-/-} genotype. The most significantly upregulated gene was *Axin-1*, a negative regulator of WNT signaling that can induce apoptosis, in the *Apoe*^{-/-}*Mif*^{-/-} genotype (Figure S9). Interestingly, *Col4a4*, which encodes for type IV collagen, a collagen form present in the endothelial basement membrane and in plaques near the fibrous cap and suggested to control VSMC phenotype switching,⁵² was among the highest upregulated genes in the *Apoe*^{-/-} genotype (Table S6).

Finally, 549 genes were differentially expressed when comparing between the 24-week and 42-week HFD group of *Apoe*^{-/-}*Mif*^{-/-} mice (Figure 4C,D and Table S5). The top significant enriched gene in 42-week HFD *Apoe*^{-/-}*Mif*^{-/-} mice was *Aldh6a1*, the gene encoding for the esterase methylmalonate semialdehyde dehydrogenase, but nothing is known yet about links between this gene and cardiovascular or inflammatory diseases. Similarly, top elevated *Hlf*, the gene encoding for hepatic leukemia factor, a member of the PAR bZIP family, has not been linked to atherosclerosis or inflamm'aging. In line with the data of the 24-week HFD comparison, *Thrsp* and *Plin1* showed up among the top genes enriched in the 42-week HFD group of *Apoe*^{-/-}*Mif*^{-/-} mice as well (Figure 4E,F and Table S5). Other potentially interesting top enriched genes in this group were *Cpne7*, a gene related to the “lipid biosynthesis” cluster of pathways (Figure 4F), a Ca²⁺-dependent, phospholipid-binding protein that is highly elevated in certain T cells and has been implicated as inflammation amplifier,⁵³ as well as *Il34* (Figure 4C,F and Table S5), the gene for interleukin-34, the alternate ligand of the CSF-1 receptor CSF1R, with important functions in monocyte proliferation and migration.⁵⁴

Together, the RNA-Seq comparison of mRNAs from BCA plaque sections of *Apoe*^{-/-}*Mif*^{-/-} and *Apoe*^{-/-} mice after 24 and 42 weeks of HFD revealed a MIF- and aging/HFD duration-dependent transcriptomic signature with lipid metabolism and immune pathways as well as genes with implicated roles in lipid synthesis, lipid storage, foam cell formation, macrophages, T cells, and brown adipose cell differentiation. The highly significant changes

in *Tnnt3* (and *Tnnt2*) and the enrichment in muscle contraction-related pathways might points toward an influence on VSMC activity.

3.5 | *Mif*-deficient mice exhibit a distinct plasma cytokine/chemokine signature that changes upon aging

As MIF is a well-known upstream modulator of inflammatory cytokines such as tumor necrosis factor- α (TNF- α), IL-1 β , or CCL2^{7,9,12} and as cytokines are key markers of aging-related changes in atherosclerosis (“inflamm'aging”),²⁶ we next profiled changes in cytokine/chemokine patterns between the *Apoe*^{-/-} and *Apoe*^{-/-}*Mif*^{-/-} genotypes at 24 versus 42 weeks of HFD using a Luminex-based multiplex approach. Using the ProcartaPlex Mouse Cytokine and Chemokine 1A 36-Plex panel, 36 cytokines and chemokines were quantified in plasma from six mice per group. Quantifiable signals above threshold were obtained for 31 cytokines/chemokines. Various MIF- and aging-dependent changes in the cytokine/chemokine pattern were detected. Overall, as illustrated by the heatmap, numerous inflammatory cytokines and chemokines were found to be downregulated in *Apoe*^{-/-}*Mif*^{-/-} mice after 24 weeks of HFD compared with the respective *Mif*-proficient *Apoe*^{-/-} control group. By contrast, a much lesser or no relative down-regulation was determined for these mediators after 42 weeks of HFD, while some cytokines exhibited a comparable pattern of down-regulation in the *Mif*-deficient genotype at 24 and 42 weeks HFD (Figure 5A). Some cytokines/chemokines appeared to be relatively upregulated in the *Mif*-deficient group at 42 weeks HFD, when compared to the corresponding change at 24 weeks HFD. Significant changes were detected for the pro-inflammatory chemokines CXCL1, CCL2, CCL7, and CCL11, the pro-inflammatory cytokines TNF- α , M-CSF, and IL-5, as well as the anti-inflammatory cytokine IL-10 (Figure 5B, Figure S10). The plasma levels of CXCL1, CCL2, and CCL11 were significantly reduced in *Mif*-deficient mice at 24 weeks HFD, whereas *Mif*-dependent differences for these inflammatory chemokines were lost after 42 weeks HFD; similarly, TNF- α in plasma from *Mif*-deficient mice exhibited a trend for a decrease at 24 weeks HFD, but no difference between the 42-week groups. The levels of CCL7 and M-CSF were decreased in *Mif*-deficient mice in both aging groups, while IL-5 was elevated in the plasma of *Mif*-deficient mice, and this effect was significant in the 42-week group. Levels of the anti-inflammatory cytokines IL-10 did not differ between *Apoe*^{-/-}*Mif*^{-/-} mice and *Apoe*^{-/-} mice at 24 weeks HFD, but—as expected—were downregulated in the *Mif*-deficient mice in the 42-week

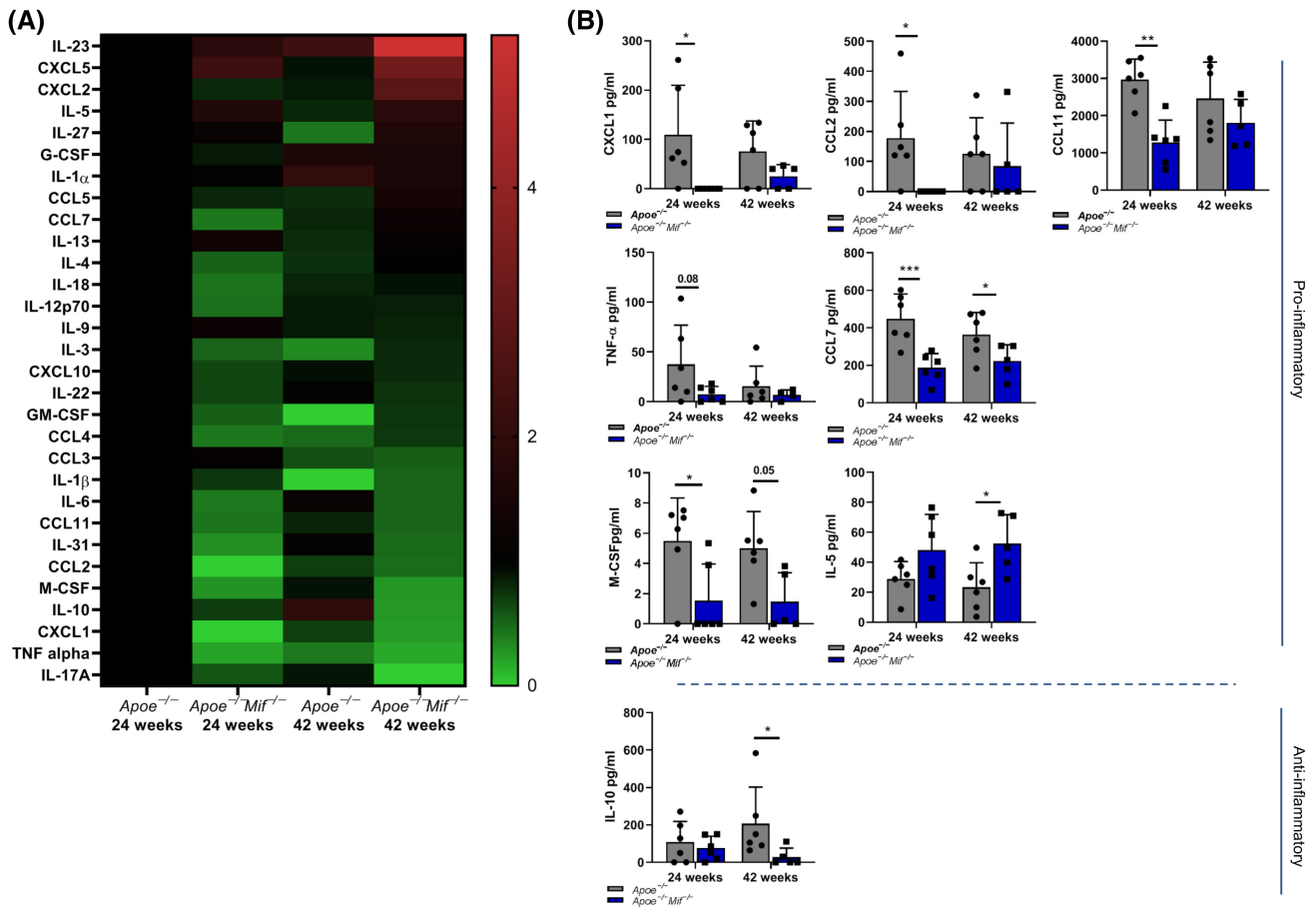


FIGURE 5 *Mif* deficiency attenuates pro-inflammatory cytokines in *Apoe*^{-/-} mice on HFD for 24 weeks but not after 42 weeks of HFD. Thirty-six cytokines and chemokines in the plasma of *Apoe*^{-/-}*Mif*^{-/-} and *Apoe*^{-/-} mice after 24- versus 42 weeks of HFD were quantified by Luminex multiplex technology. Of 36 cytokines/chemokines represented in the ProcartaPlex Mouse Cytokine and Chemokine, 31 provided measurable levels above detection threshold. (A) Normalized values of cytokine and chemokine concentration are shown in the heatmap. Mean of cytokine concentration was taken from each group, followed by normalizing each group to *Apoe*^{-/-} mice with 24 weeks of HFD. Therefore, all the cytokines from *Apoe*^{-/-} with 24 weeks HFD are normalized to 1 (first column, black). Compared to the 24-week HFD *Apoe*^{-/-} control group, upregulated cytokines are shown in red, while downregulated cytokines are shown in green. (B) Upper panel: pro-inflammatory cytokines are downregulated in the 24-week HFD *Apoe*^{-/-}*Mif*^{-/-} mice (left, blue) in comparison with 24-week HFD *Apoe*^{-/-} mice (left, gray), but the decrease in these pro-inflammatory cytokines is attenuated or disappears along with aging (42-week HFD groups; *Apoe*^{-/-}*Mif*^{-/-} mice (right, blue), *Apoe*^{-/-} mice (right gray). Lower panel: the anti-inflammatory cytokine IL-10 increases across aging/HFD, but *Mif* deletion suppresses this aging/HFD-induced increase in IL-10. Bars shown represent data from *n* = 6 independent mice and results are shown as means \pm SD. Statistics: two-way ANOVA with Sidak's multiple comparisons test. **p* < .05; ****p* < .001; *****p* < .0001, nonsignificant results with *p*-values between .05 and .1 are indicated.

group (Figure 5B). RT-qPCR measurements of aortic expression levels of IL-1 β , IFN- γ , IL-6, and CXCL1 further confirmed the down-regulation of prominent inflammatory mediators in the *Mif*-deficient group at 24 weeks of HFD (Figure S11).

Thus, overall, *Mif*-deficient aged mice exhibited a distinct plasma cytokine/chemokine signature consistent with the notion that some key inflammatory cytokines and chemokines are downregulated in *Mif*-deficient mice after 24 weeks of HFD and that such mediators are either not downregulated or even upregulated in *Mif*-deficient aged mice compared with the corresponding younger ones.

3.6 | Association of *Mif* deficiency and aging with lymphocyte-rich cell clusters and anti-oxLDL antibody levels

The above-described data suggest that changes in lesional macrophages and T cells in combination with alterations in lesional transcriptomic and plasma cytokine signatures are important determinants of the observed *Mif*- and age-dependent plaque phenotypes. One additional, potentially *MIF*-dependent mechanism may involve peri-adventitial lymphocyte-rich cell clusters that have recently been

implicated in the course of studies linking MIF and B cells in atherosclerosis.^{23,55} We therefore next determined such cell clusters in the BCA over the course of aging.

After 24 weeks of HFD, we observed peri-adventitial leukocyte clusters, reminiscent of lymphocyte/B-cell-rich clusters, in the BCA of *Apoe*^{-/-}*Mif*^{-/-} mice, while such clusters were rare in age-matched *Apoe*^{-/-} controls (Figure 6A,B). Interestingly, this relative difference in

cluster abundance disappeared in aged mice that received HFD for 42 weeks, as the number of clusters increased in *Apoe*^{-/-} mice at this aging stage (Figure 6B). Thus, *Mif* deficiency leads to an increase in cluster numbers in medium-aged hyperlipidemic *Apoe*^{-/-} mice, but this difference is lost toward more advanced aging stages. We next characterized the nature and cellular composition of the clusters. Adventitial immune cell aggregates have

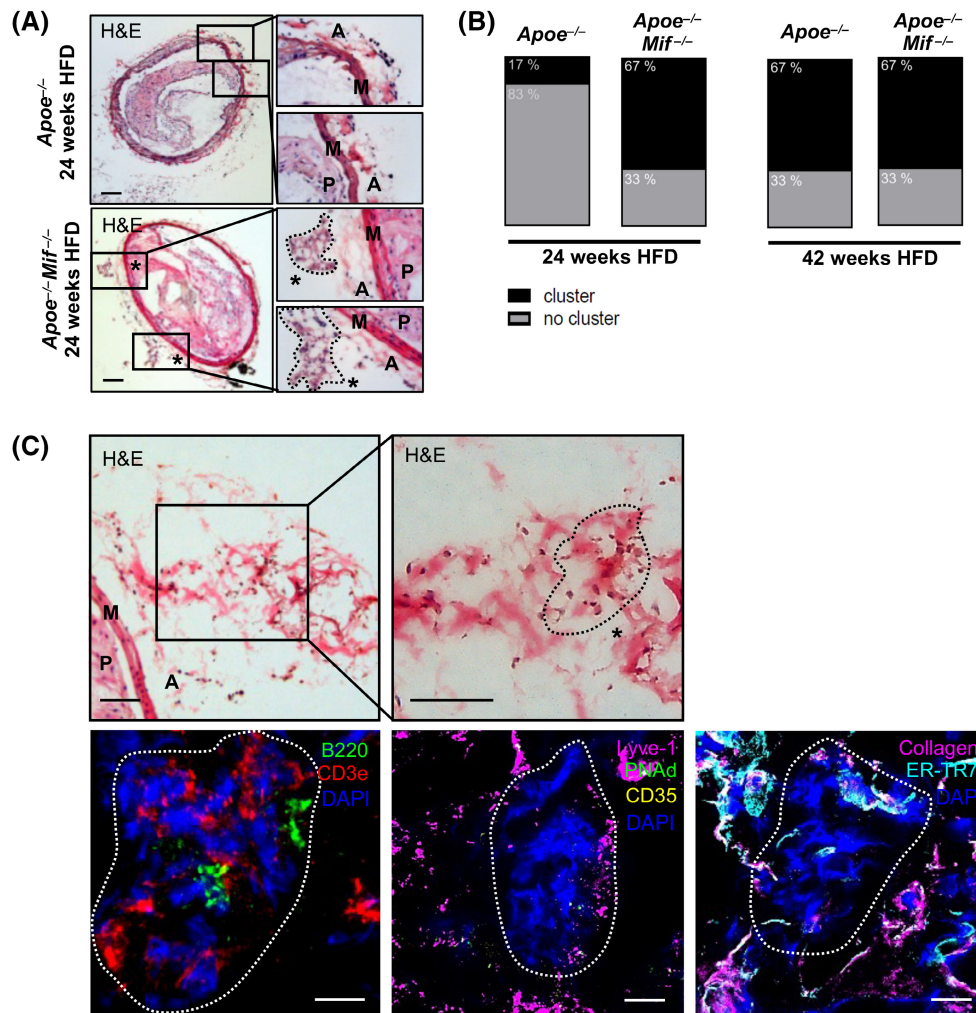


FIGURE 6 *Mif* deficiency accelerates the formation of peri-adventitial lymphocyte-rich clusters. (A,B) Detection of lymphocyte-rich (peri-)adventitial cell clusters in the BCA of *Mif*-deficient versus *Mif*-expressing hyperlipidemic *Apoe*^{-/-} mice. (A) Representative images of lymphocyte-rich (peri-)adventitial cell clusters in the BCA of 30-week-old *Apoe*^{-/-} control mice (upper panel) versus *Apoe*^{-/-}*Mif*^{-/-} mice (lower panel) on HFD for 24 weeks as assessed by H&E-staining. A total of 10 serial sections with a distance of 50 μm were screened for lymphocyte-rich (peri-)adventitial cell clusters for each mouse. Boxed areas containing lymphocyte-rich (peri-)adventitial cell clusters (lower panel) or no clusters (upper panel) are also shown at higher magnification (right-hand panels). Cell clusters in the boxed areas of the lower panel are indicated by an asterisk and circled in the enlarged panels. A = adventitia, M = media, P = plaque, scale bar: 100 μm. (B) Quantification of the detected lymphocyte-rich (peri-)adventitial cell clusters comparing *Apoe*^{-/-}*Mif*^{-/-} and *Apoe*^{-/-} mice at both the 30/24 and 48/42 age/HFD time intervals ($n = 6$ mice per group). (C) The lymphocyte-rich (peri-)adventitial cell clusters in *Mif*-deficient *Apoe*^{-/-} mice stain for markers that are also found in stage I ATLOs. Representative images of the immunostaining of the clusters against ATLO-related markers (lower panel) including B220 (B cells), CD3e (T cells), LYVE-1 (lymphatic vessel endothelial hyaluronic acid receptor 1; lymph vessels), PNA (peripheral node addressin; high-endothelial venules), CD35 (follicular dendritic cells), ER-TR7 (reticular fibers/fibroblasts), and collagen IV (scale bar: 10 μm). For a better visualization of the localization of the clusters, the H&E images of the respective region are shown (upper panel). The circled region in the enlarged H&E image section marked by an asterisk indicates the analyzed cluster (scale bar: 50 μm).

been discussed in the context of sustained chronic inflammation and the formation of ATLOs in aged atherogenic *Apoe*^{-/-} mice.²⁷ Thus, we determined whether the identified peri-adventitial cellular clusters in *Mif*-deficient mice would have features of adventitial ATLOs. Due to their T- and B-cell-rich lymphoid organ-like structure, ATLOs can be identified through a variety of markers, including those for lymphocytes, lymph vessels, high-endothelial venules (HEVs), and capsule components. Using anti-CD3e and anti-B220 antibodies, we detected the presence of T and B cells, respectively, in peri-adventitial clusters of *Apoe*^{-/-}*Mif*^{-/-} mice (Figure 6C). Moreover, the clusters contained lymph vessels and conduit-like structures, as evident by pronounced staining for Lyve-1 and ER-TR7, respectively, and contained substantial collagen type IV positivity (Figure 6C). However, features of mature ATLOs were absent, as indicated by lack of staining for peripheral node addressin (PNAd), a marker of HEVs, and CD35, a marker for follicular dendritic cells (FDCs) (Figure 6C). Together, these results suggested that the lymphocyte-rich clusters that we detected in the BCA of 24-week HFD-fed *Apoe*^{-/-}*Mif*^{-/-} mice as well as the BCA of aged 42-week HFD-fed *Apoe*^{-/-}*Mif*^{-/-} and *Apoe*^{-/-} mice have similarities to early ATLOs, possibly corresponding to a stage I ATLO.²⁸ ATLO-derived B cells have been attributed atherogenesis-dampening properties possibly through atheroprotective IgM antibodies in aged *Apoe*^{-/-} mice.^{56,57} To begin to study such links in our mouse model, we analyzed the plasma levels of anti-oxLDL antibody isotypes.⁵⁸ Anti-oxLDL IgM antibody levels that have been associated with atheroprotection⁵⁸ were significantly decreased after 42 weeks of HFD in *Apoe*^{-/-}*Mif*^{-/-} mice (Figure S12). In line with these results, titers of the anti-oxLDL IgG isotype, which are associated with enhanced atherosclerosis,⁵⁸ were not decreased (Figure S12). The decrease in anti-oxLDL antibodies of the IgM isotype may contribute to the attenuation of atheroprotection seen in 42-week HFD-fed *Apoe*^{-/-}*Mif*^{-/-} mice.

4 | DISCUSSION

Macrophage migration inhibitory factor (MIF) is an inflammatory cytokine and atypical chemokine that was previously shown to promote atherogenesis by enhancing CXCR2/4-mediated leukocyte recruitment and vascular inflammation. The current study for the first time establishes a link between MIF and age-related changes in atherosclerotic pathology, demonstrating that atheroprotection in global *Mif*-gene-deficient atherogenic *Apoe*^{-/-} mice is attenuated during the course of aging and Western-type HFD. Characterization of this phenotype by peripheral, lesional, and peri-adventitial immune cell

profiles, as well as lesional transcriptomic and circulating cytokine signatures, identifies candidate mechanisms that in conjunction may determine the observed dependence on *Mif* expression across the course of aging in hyperlipidemic *Apoe*^{-/-} mice. Figure 7 summarizes these mechanisms and their potential link to *Mif* deficiency, aging, and atheroprotection.

MIF has been attributed an overall pro-inflammatory and atheroprotective role as evidenced in various experimental models of atherosclerosis applying *Mif*-gene deficiency or antibody blockade and in line with correlations between MIF expression levels and human atherosclerotic disease.^{8,10,18,20,22} However, while the specific role of the cardiac MIF/AMPK axis was examined in ischemic recovery in the senescent heart,⁴⁰ the contribution of MIF in different stages of atherosclerotic lesion formation and across aging has not been systematically studied. Here, we analyzed the influence of *Mif*-gene deficiency in *Apoe*^{-/-} mice across different ages and HFD exposure intervals. *Mif*-knockout and wildtype *Apoe*^{-/-} mice were compared at an age of 30, 42, and 48 weeks, corresponding to 24, 36, and 42 weeks of HFD treatment, respectively. To further study the influence of aging versus duration of exposure to a cholesterol-rich HFD, a model of 52-week-old mice, in which HFD was limited to the last 6 weeks, was employed.

Deletion of the *Mif*-gene in the atherogenic *Ldlr*^{-/-} mouse model leads to protection from atherosclerotic plaque formation across the entire vascular bed, including aortic root and arch.^{18,21} Protection conveyed by global *Mif* deletion in the context of the *Apoe*^{-/-} model was found to be limited to the BCA and abdominal aorta and when circulating MIF is systemically inhibited by neutralizing antibodies in *Apoe*^{-/-} mice, atherogenic inflammation is attenuated but no significant reduction in plaque burden was observed.^{22,23} The precise mechanistic causes for this background-specific difference have yet to be explored, and it is currently unclear whether a similar phenotype would be seen in conditional, cell/tissue-specific models of *Mif*-gene deletion, such as in arterial- or myeloid-specific *Mif*-knockouts. Here, we confirm the regio-specific atheroprotective effect of *Mif* deficiency in BCA and abdominal aorta in 30-week-old *Apoe*^{-/-} mice on HFD for 24 weeks. Notably, the site-specific atheroprotective effect was reduced or “lost” in 48-week-old *Mif*-deficient mice on HFD for 42 weeks, as well as in 52-week-old mice that had been on HFD for the last 6 weeks. An observed reduction in plasma triglycerides, but not cholesterol, in the 48-week-old *Mif*-deficient mice compared with their 30-week-old counterparts argues against the possibility that systemic effects on lipid regulation are the main cause for the observed age-dependent effect, but, interestingly, comparing the transcriptomic profile of plaque tissue between 48- and 30-week-old *Mif*-deficient mice showed

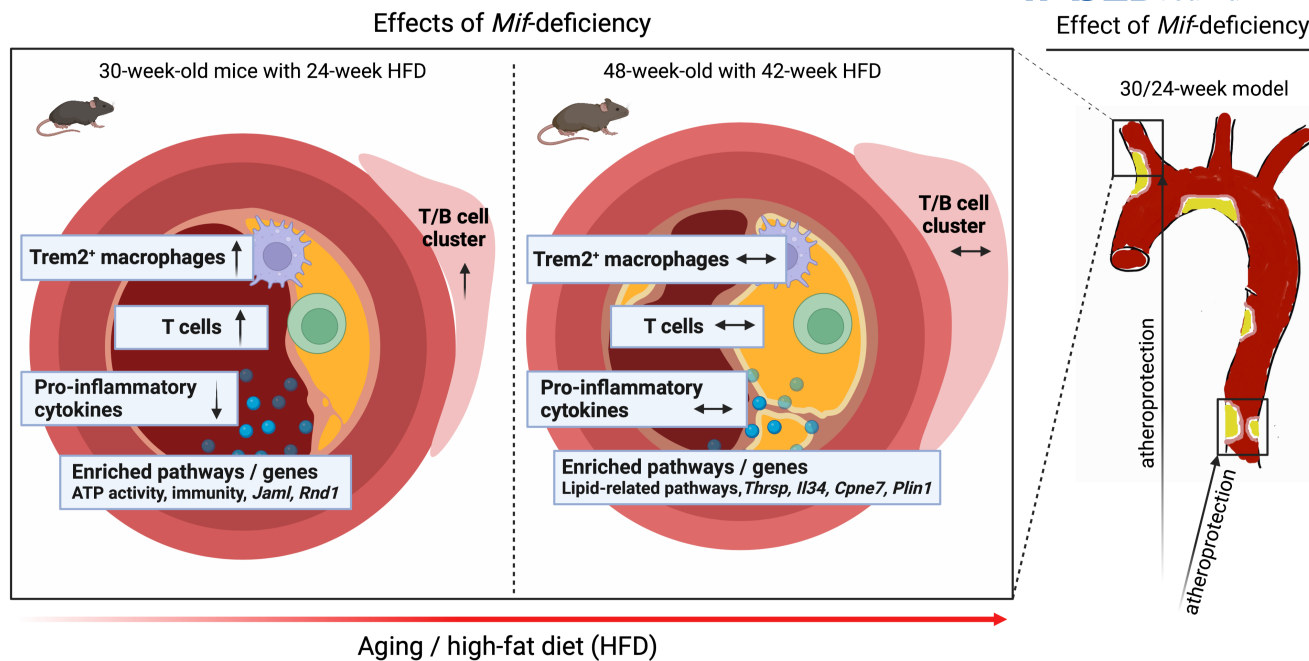


FIGURE 7 Scheme summarizing the age- and MIF-dependent effects in advanced atherosclerosis. The scheme summarizes the effects of global *Mif*-gene deficiency in 30- and 48-week-old *Apoe*^{-/-} mice that received HFD for 24 and 42 weeks, respectively. Lack of MIF was accompanied by atheroprotection in the BCA and abdominal aorta in the 30/24-week group (left-hand vessel image), an effect that was attenuated in the more aged 48/42-week group (right-hand vessel). The atheroprotective phenotype of *Mif*-gene deletion in the 30/24-week group was paralleled by an increase in lesional Trem2⁺ macrophages and lesional CD3⁺ T cells. Not separately depicted in the graph is the observed increase in splenic CD4⁺ T cells in this group and the inverse reduction in blood CD4⁺ T cells. The protective plaque phenotype in the *Mif*-deficient 30/24-week group was furthermore accompanied by a less inflammatory cytokine signature and a higher number in peri-adventitial lymphocyte-rich clusters. All these effects were attenuated or lost in the 48/42-week *Mif*-deficient group. The atheroprotective phenotype seen in *Mif*-deficient mice on a 24-week HFD was furthermore accompanied by a transcriptomic signature, for example, featuring enrichment of ATP-dependent activity and contractile cell pathway features (ATP), regulation of myeloid leukocyte-mediated immunity (immunity), or the genes *Jaml*, a junctional adhesion molecule, *Rnd1*, a Rho family GTPase. On the contrary, the phenotype of *Mif*-deficient mice on a 42-week HFD was accompanied by an enrichment of lipid-related pathways and genes such as *Thrsp*, *Il34*, *Cpne7*, and *Plin1*. HFD, high-fat diet; Trem2, triggering receptor expressed on myeloid cells 2; *Jaml*, junctional adhesion molecule-like; *Rnd1*, Rho family GTPase 1; *Thrsp*, thyroid hormone-responsive spot 14; *Il34*, interleukin-34; *Cpne7*, copine variant 7; *Plin1*, perilipin-1. The cartoon was generated with www.BioRender.com.

that several “lipid-related pathways” were among the most enriched pathways in the older *Mif*-deficient group.

We propose a differential role of *Mif* deficiency on the abundance and activity of circulating and lesional immune cells, foam cells, as well as inflammatory status across aging and atherosclerosis stages, unleashing certain suppressed mechanisms that are atheroprotective in aggregate, and that become attenuated upon aging. This may be linked to an overall increased inflammatory status in the more aged atherosclerotic mice. In fact, inflammatory cytokine levels such as those of IL-6, TNF- α , or IL-1 β have been found to increase over the course of aging (“inflamm’aging”) and have been suggested to contribute to aging-related exacerbation of atheroprotection as both vascular extrinsic and intrinsic factors.^{59–61} In overall agreement with this notion, our cytokine profiling analysis revealed that key inflammatory cytokines and chemokines were downregulated in *Mif*-deficient mice in the

24-week but not in the 42-week HFD group. Furthermore, the overarching cytokine heatmap illustrates that a higher number of inflammatory cytokines and chemokines is downregulated in a more pronounced manner in the 24-week *Mif*-deficient group compared with *Apoe*^{-/-}*Mif*^{-/-} mice on HFD for 42 weeks. Inversely, more inflammatory mediators display similar or even upregulated levels in the 42-week *Mif*-deficient group. The mechanistic details are likely complex and not linearly dependent on MIF expression and circulating MIF levels. To this end, we determined MIF mRNA expression levels in spleen and liver and MIF protein levels in plasma in our mouse model, but did not detect any differences between the 24- and 42-week HFD groups. One study in humans suggests an increase in circulating MIF levels in the elderly,⁶² whereas age-related tissue expression of murine MIF was found to be increased in aorta⁶³ but decreased in cardiac tissue.⁴⁰ Overall, age-related changes in systemic/peripheral MIF

expression levels cannot readily explain the observed loss of atheroprotection in the aged *Mif*-deficient animals, supporting the notion that local vascular MIF levels might be more relevant in contributing to the observed aging-related phenotypes.

We noted an effect of *Mif* deletion on lesional macrophages and T cells, which was lost upon aging. Compared with *Apoe*^{-/-} controls, *Mif*-deficient *Apoe*^{-/-} mice exhibited higher lesional macrophage and T-cell counts in 30-week-old animals after 24 weeks of HFD, but no difference was apparent any longer in the aged 48/42-week mice. This appeared to be mainly due to a drop in relative numbers of these cells in *Mif*-deficient mice over the course of aging.

Interestingly, further analysis showed that the number of Trem2⁺ macrophages, a subtype for which previous studies have implicated a foamy and anti-inflammatory transcriptomic signature,^{41,43} was elevated in *Mif*-deficient mice in the 24-week HFD group and significantly decreased between the 30/24 and 48/42 time points. A relationship between MIF and foamy macrophages is also supported by our transcriptomics data, as fatty acid biosynthesis, lipid storage, and lipoprotein regulation are among the top-enriched pathways in 24-week HFD wildtype and 42-week HFD *Mif*-deficient *Apoe*^{-/-} mice. Moreover, *Plin1*, *Thrsp*, and *Ldlr* were among the highest enriched genes in the 24-week HFD *Apoe*^{-/-} mice. Of note, systemic or bone marrow deficiency of *Plin1* was previously found to attenuate atherosclerotic lesions⁶⁴; *Thrsp* is a regulator of lipogenesis⁴⁸; hepatic LDLR controls plasma LDL-cholesterol, but LDLR also is involved in MIF-mediated macrophage uptake of native LDL.⁴⁹ Together, this suggests that MIF may contribute, at least partially, to the abundance and phenotype of foamy macrophages in the BCA lesions and that their changes may play a role in age-dependent attenuation of atheroprotection in *Mif*-gene-deficient mice. Although causality has not yet been demonstrated for Trem2⁺ macrophages in atherosclerosis, it is of note that their insinuated anti-inflammatory transcriptomic signature parallels their increased lesional content in *Mif*-deficient mice in the 24-week HFD group, which in turn is associated with an overall less inflammatory circulating cytokine/chemokine signature. In this context, arterial immune cell infiltration/content as a vascular intrinsic factor has been linked to the effects of aging on vascular inflammation and lesion formation.^{59,65,66} Using an *Ldlr*^{-/-} model of atherosclerosis, it was additionally shown that aging in combination with HFD induces monocytosis and aortic macrophage accumulation.⁶⁷ However, how aging affects immune cell numbers specifically in the BCA of *Apoe*^{-/-} mice has not been investigated. Our data suggest that MIF could serve as a regulator of immune cell homeostasis in the BCA,

suppressing—either directly or indirectly—macrophage subpopulations such as the foamy/Trem2⁺ subtype. Our quantification of plaque Trem2⁺ Ki67⁺ cells and proliferating Edu⁺Trem2⁺ BMDMs indicates that this could be due to an effect on the proliferative capacity of lesional Trem2⁺ cells. Accordingly, MIF might contribute to an imbalance between macrophage subtypes, overall promoting atherosclerotic plaque formation, a property that is lost or overridden in the course of aging. MIF may thus display a dichotomic and biphasic role in the atherogenic vasculature. While it primarily promotes leukocyte infiltration and vascular inflammation in young and middle-aged mice through its chemokine-like inflammatory activities as shown in numerous studies,^{10,18,20,21,39} and may attenuate the proliferation of plaque macrophage subtypes such as Trem2⁺ macrophages; these effects may be attenuated or become overcompensated in the aged vessel wall. The transcriptomic data add important pathway information in this regard. In addition to the enriched lipid biosynthesis, storage, and lipoprotein pathways including genes such as *Plin1*, *Plin4*, *Ldlr*, or *Thrsp* (see above), the transcriptomics data revealed that the alternative M-CSF receptor agonist *Il34* is upregulated in *Mif*-deficient mice after 42 weeks of HFD in comparison with the *Mif*-deficient 24-week HFD control group. *Plin1* and *Il34* have previously been shown to be higher in patients with coronary heart disease with a hemodialysis and heart failure background, respectively, indicating they may have roles in atherogenic diseases. Furthermore, *Plin1* enhances CD36 expression and inhibits cholesterol ester hydrolysis inside macrophages promoting foam cell formation, while systemic or myeloid *Plin1*-deficient mice exhibited an attenuation of plaque size in aortic root; IL-34 also enhances foam cell formation via upregulating CD36 expression on macrophages and promoting oxLDL uptake.^{64,68–70} To this end, it is interesting to note that the Luminex data showed that *Mif* deficiency led to a down-regulation of circulating M-CSF, although no aging/HFD-dependent difference was observed. Furthermore, the observed enrichment of the TP53-regulated cell death gene pathway in the 24-week HFD *Mif*-deficient group provides further links to foam cells and inflammation. A potential effect could involve the stabilization of plaque macrophages by apoptosis reduction.⁷¹ A detailed future investigation of MIF effects on the recruitment, survival, or polarization of selective vascular wall macrophage subpopulations, including the involved MIF receptor pathways, would thus be warranted. Interestingly, we also observed an influence of MIF on T cells. Immunofluorescence staining and qPCR showed that lesional CD3⁺ T-cell numbers were elevated in *Mif*-deficient *Apoe*^{-/-} mice after 24 weeks of HFD compared with control group, but no such difference was seen after 42 weeks of HFD. Furthermore, splenic CD4⁺

T-cell numbers in *Apoe*^{-/-}*Mif*^{-/-} mice were significantly increased both at 24 and 42 weeks of HFD compared to T-cell numbers in spleens from *Apoe*^{-/-} mice. It is well established that aging affects the anatomy and organization of the spleen.⁷² Also, different studies have revealed a lowered abundance of splenic T-cell zones in aged C57BL/6 mice that was accompanied by a reduction in CD4⁺ T-cell recruitment and function^{16,73} and that T-cell aging induces T-cell activation but decreases peripheral T-cell numbers.^{74,75} The result also may be suggestive of a T-cell retainment effect of *Mif* deficiency in lymphoid organs. Mechanistically, lack of a functional MIF/CXCR4 axis in the *Mif*-deficient mice might account for the apparent retainment of T cells in spleen. Future studies would be warranted to test this hypothesis applying *Mif*-deficient mice, MIF or CXCR4 inhibitors such as AMD3100 or ms-R4M-L1, or even conditional models with, for example, *Cxcr4*-deficient T cells, as well as recruitment experiments.

Moreover, aging plaque T cells can accumulate cholesterol, a mechanism that has been suggested to promote T-cell apoptosis and senescence, while attenuating atherosclerosis.⁷⁶ Our transcriptomic analysis identified *Cpne7*, the gene that encodes for copine-7, a member of the copine family of proteins, to be downregulated in *Mif*-deficient 24-week HFD mice and highly upregulated in the 42-week *Mif*-deficient group. Copins are a poorly characterized group of Ca²⁺-dependent, phospholipid-binding proteins that are thought to play a role in membrane-trafficking processes.⁷⁷ Interestingly, only a few cell types express *Cpne7*. Within the immune cell compartment, it is highly expressed in T cells, in particular in mucosal-associated invariant T (MAIT) cells and memory CD4⁺ T cells (<https://www.proteinatlas.org/ENSG00000178773-CPNE7/single+cell+type>). MAIT T cells are unconventional T cells with innate-like antimicrobial activity but have also been assigned various deleterious and protective functions in autoimmune, inflammatory, and metabolic diseases⁷⁸ and might thus play a role in the atherogenic vasculature. *Cpne7* has not been investigated in the context of atherosclerosis, but the inner mass cells from vulnerable carotid atherosclerotic plaques express higher *Cpne7* levels than the ones from stable plaques, inferring that *Cpne7* might have a role in the progression of atherosclerosis.⁷⁹

We did not observe changes in BCA plaque VSMC numbers, but notably, *Col4a1* and *Tnnt3* (as well as *Tnnt2*), were among the top-enriched genes in our transcriptomic analysis, indicating effects on VSMC phenotype. *Col4a1* was highly enriched in the 24-week *Mif*-deficient mice as well as in the 42-week paradigm, when comparing *Mif*-expressing to *Mif*-deficient mice. *Tnnt3* was the top-enriched gene in the 24-week treatment group in the *Mif*-expressing genotype. Together, their known roles in basement membrane stabilization, VSMC phenotype, and

contractility, insinuate that the *Mif* genotype and aging may affect VSMC plasticity, an important mechanism controlling plaque inflammation and stability.⁸⁰ Currently, only one report has directly probed causal links between MIF and VSMC phenotype switching.⁸¹

We previously observed an enhanced re-organization of B cells into cluster-like structures in peri-adventitial areas in proximity to atherosclerotic plaques in the BCA of *Mif*-deficient *Apoe*^{-/-} mice.²³ Here, we show that the formation of lymphocyte-rich clusters in *Apoe*^{-/-} mice is age-dependent and that *Mif* deficiency accelerated the formation of the clusters at 24 weeks of HFD, an effect that paralleled the attenuation of lesion formation due to *Mif* deficiency. We also noted that the increase in cluster numbers in *Mif*-deficient mice compared to *Mif*-expressing controls vanished during the course of aging. We provide evidence that the clusters that form in an accelerated manner in *Mif*-deficient *Apoe*^{-/-} mice show features reminiscent of stage I or early-stage ATLOs. Adventitial ATLOs are typically observed in highly aged *Apoe*^{-/-} mice on chow for 52–78 weeks. ATLOs display a lymphoid-like organ structure with organized T- and B-cell zones including germinal centers (GCs), lymph vessels, high-endothelial venules, and follicular dendritic cells (FDCs).^{28,82} Based on the expression of various markers, ATLOs of different maturation stages, that is, stage I, II, and III, can be classified.^{28,83} Moreover, ATLOs need to be differentiated from fat-associated lymphoid clusters (FALCs), which are T/B-cell aggregates that are exclusively observed in adipose tissue.²⁸ Stage I ATLOs feature loosely arranged B and T cells and lymphocytes in these early ATLOs are not organized in dedicated B- and T-cell areas. They are also characterized by the expression of lymphorganogenic chemokines such as CXCL13. Stage II ATLOs contain separate T- and B-cell areas and lymph vessel neogenesis becomes prominent together with a dense network of lymph node-like conduits connecting the arterial wall with newly formed HEVs. By contrast, fully matured or stage III ATLOs display separate T-cell and B-cell follicles, activated germinal centers (GCs) with FDCs, plasma cell (PC) niches, lymph vessels, as well as blood vessel neogenesis. In addition to an accumulation of B and T cells, we detected a vascular system including LYVE-1⁺ lymphatic vessels, and appreciable collagen IV expression. However, organization of the infiltrated lymphocytes into clearly distinct T- and B-cell zones as well the formation of GCs with FDCs that is characteristic of stage II/III ATLOs were absent.²⁸ As our structures only contained sparse ER-TR7 positivity, we conclude that they are distinct from secondary lymphoid organs (SLO), which would exhibit a well-structured ER-TR7⁺ encapsulation.²⁸

The functional role of ATLOs in atherosclerosis is incompletely understood. However, recent data revealed an

atheroprotective role accompanied by activation of anti-inflammatory Treg cells within the ATLO.⁵⁶ Moreover, different B-cell subsets have been described to be present in ATLOs with B1b B cells representing the majority of the B-cell compartment.⁵⁷ B1 cells have been attributed atheroprotective functions by secreting natural IgM.^{84,85} These immune cells in ATLOs express different neuronal receptors for adventitia innervating sympathetic and sensory neurons for bidirectional neuroimmune interactions and form neuroimmune cardiovascular interfaces to regulate atherosclerosis progression.²⁹ We would hypothesize that our identified peri-adventitial lymphoid-rich cell clusters may contribute to the atheroprotective effect in *Mif*-deficient *Apoe*^{-/-} mice that is eventually attenuated during aging. This notion is further supported by an observed reduction in circulating atheroprotective anti-oxLDL IgM levels, whereas anti-oxLDL IgG levels remained unchanged. Natural IgM-type antibodies are considered atheroprotective, while IgG antibodies are generally viewed as atheroprotective.⁵⁸ Anti-oxLDL IgM antibodies have been shown to neutralize oxLDL and inhibit its uptake by macrophages thereby suppressing foam cell formation, whereas anti-oxLDL IgG antibodies form complexes with oxLDL that promote lesional macrophage activation via Fcγ-receptors.⁵⁸

Perivascular adipose tissue (PVAT) is another peri-adventitial cell cluster known to communicate with cells in the atherosclerotic plaque and known to have a profound regulatory role in controlling vascular inflammation.^{86,87} In this context, the identification of pathways related to brown adipose cell differentiation by our transcriptomic analysis could be notable. The “brown adipose cell differentiation” pathway was top-enriched in 24-week *Apoe*^{-/-} compared to *Apoe*^{-/-}*Mif*^{-/-} mice as well as in 42-week *Apoe*^{-/-}*Mif*^{-/-} compared to *Apoe*^{-/-} mice. While only one previous study indirectly points to an influence of MIF on brown adipose tissue (BAT),⁸⁸ the transcriptomic data suggest that MIF and aging may contribute to PVAT phenotype changes leading to an increased or attenuated (“being”) inflammatory status, with consequences for the adjacent plaque tissue.

Our study of *Mif* deficiency in the context of atherosclerosis and aging furthers the notion that aging affects atherogenesis in a complex manner, with cytokine/chemokine-related inflammatory mechanisms playing key roles. Considering the continuing rise of atherosclerotic patients in an aging population, the design of treatment strategies specifically tailored for elderly individuals will become important. Based on the principal success of the CANTOS trial⁸⁹ and the emerging link between inflamm'aging and atherosclerosis,²⁶ cytokine/chemokine-directed strategies may represent promising approaches for age-tailored intervention strategies. MIF is a promising

target in atherosclerosis and a variety of inhibition routes including antibody-, small molecule-, and peptide-based strategies have been discussed.^{9,90,91} However, age-tailored strategies have not been investigated. The preclinical data obtained in our present study confirm numerous previous studies suggesting that MIF-based inhibition strategies may be promising in cardiovascular patients. The “attenuated-atheroprotection phenotype” related to *Mif* deficiency and advanced aging was observed in global *Mif*-gene-deficient mice. Global gene deficiency may cause various compensatory mechanisms and MIF has been assigned both extracellular inflammatory and intracellular homeostatic activities.⁷ Moreover, the MIF-homolog D-dopachrome tautomerase (D-DT)/MIF-2 shares some activities with MIF,⁹² while distinct effects have also been noted.⁹³ Preliminary work suggests a role for MIF-2 in atherosclerosis.⁹⁴ Also, it would thus be interesting to test whether the observed “attenuated-atheroprotection phenotype” seen in the context of global *Mif* deficiency, is recapitulated in conditional cell/tissue-specific *Mif*-gene-deficient models, or upon MIF depletion by a pharmacological strategy. Furthermore, it may be argued that general MIF-blocking strategies might be suboptimal in highly aged individuals and that instead, receptor pathway-specific MIF-targeting strategies should be considered.⁹¹ The characterization of lesional transcriptomic and circulating cytokine signatures provided by our present study offers potential candidates for future biomarkers and may provide valuable guidance for future tailored anti-MIF strategies.

Potential specific limitations of the current study are: (i) the use of global *Mif*-gene-deficient mice; (ii) the confinement to the *Apoe*^{-/-} mouse model with its regio-specific phenotype that is not observed in *Mif*^{-/-}*Ldr*^{-/-} mice^{18,21}; (iii) the according comparison between BCA and aortic root or arch lesions; (iv) partly limited animal numbers and no confirmation in a second independent set of cohorts, owing to the long study times, drop-outs, technical challenges in BCA and peri-adventitial cluster preparations, and 3R rule considerations; (v) an analysis of metabolic changes was not systematically performed; although, with the exception of triglyceride levels at 42 weeks HFD, no significant differences were noted for body weight, cholesterol, or blood counts, the present study may warrant future studies on links between MIF, aging, and metabolism to identify potential metabolic alterations in the course of atherosclerosis; (vi) Treg numbers in plaques or lymphoid cell clusters could not be determined due to their low abundance; also our assessment of splenic Treg numbers only relied on qPCR for FoxP3, while additional markers such CD25 or Treg subset markers could not be determined.

In conclusion, this work has unraveled a previously unknown link between *Mif* deficiency, atheroprotection, and

aging in the *ApoE*^{-/-} model of atherosclerosis. We provide candidate mechanisms and transcriptional and cytokine signatures for the phenotype observed. While the mechanistic details of these effects and the study of a potential causality for the implicated cell types and pathways will have to be subject to future scrutiny, our study provides valuable information that further our understanding of the roles of MIF, cytokines, and inflamm'aging in atherosclerosis.

AUTHOR CONTRIBUTIONS

Jürgen Bernhagen and Christine Krammer conceived and designed the study with help from Sarajo Mohanta, Corinna Schmitz, Omar El Bounkari, Heidi Noels, Aphrodite Kapurniotu, Ozgun Gokce, and Christian Weber. Christine Krammer, Bishan Yang, Sabrina Reichl, Hao Ji, Simon Besson-Girard, Verena Bolini, and Sarajo Mohanta performed research and analyzed data. Christine Krammer, Bishan Yang, Simon Besson-Girard, Sabrina Reichl, Kai Schlepckow, Omar El Bounkari, Heidi Noels, Ozgun Gokce, Sarajo Mohanta, and Jürgen Bernhagen contributed to the interpretation of the data. The first draft of the manuscript was written by Jürgen Bernhagen, Christine Krammer, and Bishan Yang. All authors revised and commented on the manuscript drafts. Sarajo Mohanta, Kai Schlepckow, Georg Jocher, Georg Werner, Michael Willem, Christian Weber, Heidi Noels, and Corinna Schmitz contributed to critical materials, and Jürgen Bernhagen, Christian Weber, Ozgun Gokce, and Aphrodite Kapurniotu provided the funding for the study.

ACKNOWLEDGMENTS

This work was supported by Deutsche Forschungsgemeinschaft (DFG) grant SFB1123-A3 to J.B. and A.K., SFB1123-A1 to C.W., SFB1123-Z1 to S.M., SFB-TRR219-M05 to H.N., and by DFG under Germany's Excellence Strategy within the framework of the Munich Cluster for Systems Neurology (EXC 2145 SyNergy—ID 390857198) to J.B., O.G., and C.W., and LMUexc strategic partnerships to J.B. C.W. is Van de Laar Professor of Atherosclerosis. We thank Simona Gerra and Priscila Bourilhon for the technical support. We thank Christian Haass for providing access to APP/PS1 and APP/PS1*Trem2^{-/-} mice. The APP/PS1 colony was established from a breeding pair kindly provided by Mathias Jucker (Hertie Institute for Clinical Brain Research, University of Tübingen and DZNE Tübingen). The authors thank Marco Colonna (Washington University, School of Medicine) for the Trem2^{-/-} mice. We also thank Xianyuan Xiang for initial help with the Trem2 antibody staining procedure; Marlies Zarwel for helpful discussions; and Sabrina Pagano, Nicolas Vuilleumier, and Sabine Steffens for advice regarding anti-oxLDL immunoassays. We are grateful to the mouse core facility of the Center for Stroke and

Dementia Research (CSD) for their invaluable support with the mouse studies. Open Access funding enabled and organized by Projekt DEAL.

DISCLOSURES

J.B., C.W., and A.K. are inventors of patent applications related to anti-MIF and anti-chemokine strategies in inflammatory and cardiovascular diseases. The other authors declare that they have no competing interests.

DATA AVAILABILITY STATEMENT

All data and materials as well as software application information are available in the manuscript, the supplementary information, or are available from the corresponding author upon reasonable request. Raw RNA sequencing data and processed gene counts and variance stabilized expressions are available in the NCBI GEO database through accession number GSE221504.

ETHICS STATEMENT

Animal experiments were approved by the local authorities (animal ethics approval ROB-55.2-2532.Vet_02-18-040 of the government of Bavaria, Germany) and were performed according to the German animal protection law.


ORCID

Simon Besson-Girard  <https://orcid.org/0000-0003-1194-5256>

Omar El Bounkari  <https://orcid.org/0000-0002-3051-2096>

Aphrodite Kapurniotu  <https://orcid.org/0000-0001-6124-7232>

Sarajo Mohanta  <https://orcid.org/0000-0001-6144-4092>

Jürgen Bernhagen  <https://orcid.org/0000-0003-2996-2652>

REFERENCES

1. Virani SS, Alonso A, Benjamin EJ, et al. Heart disease and stroke statistics—2020 update: a report from the American Heart Association. *Circulation*. 2020;141:e139-e596.
2. Joseph P, Leong D, McKee M, et al. Reducing the global burden of cardiovascular disease, part 1: the epidemiology and risk factors. *Circ Res*. 2017;121:677-694.
3. Noels H, Weber C, Koenen RR. Chemokines as therapeutic targets in cardiovascular disease. *Arterioscler Thromb Vasc Biol*. 2019;39:583-592.
4. Weber C, Noels H. Atherosclerosis: current pathogenesis and therapeutic options. *Nat Med*. 2011;17:1410-1422.
5. Hansson GK, Hermansson A. The immune system in atherosclerosis. *Nat Immunol*. 2011;12:204-212.
6. Ross R. Atherosclerosis—an inflammatory disease. *N Engl J Med*. 1999;340:115-126.
7. Kapurniotu A, Gokce O, Bernhagen J. The multitasking potential of alarmins and atypical chemokines. *Front Med (Lausanne)*. 2019;6:3.
8. Burger-Kentischer A, Goebel H, Seiler R, et al. Expression of macrophage migration inhibitory factor in different stages of human atherosclerosis. *Circulation*. 2002;105:1561-1566.

9. Sinitski D, Kontos C, Krammer C, Asare Y, Kapurniotu A, Bernhagen J. Macrophage migration inhibitory factor (MIF)-based therapeutic concepts in atherosclerosis and inflammation. *Thromb Haemost.* 2019;119:553-566.
10. Zerneck A, Bernhagen J, Weber C. Macrophage migration inhibitory factor in cardiovascular disease. *Circulation.* 2008;117:1594-1602.
11. Müller II, Müller KAL, Schönleber H, et al. Macrophage migration inhibitory factor is enhanced in acute coronary syndromes and is associated with the inflammatory response. *PLoS ONE.* 2012;7:e38376.
12. Calandra T, Roger T. Macrophage migration inhibitory factor: a regulator of innate immunity. *Nat Rev Immunol.* 2003;3:791-800.
13. Tillmann S, Bernhagen J, Noels H. Arrest functions of the MIF ligand/receptor axes in atherogenesis. *Front Immunol.* 2013;4:115.
14. Adamali H, Armstrong ME, McLaughlin AM, et al. Macrophage migration inhibitory factor enzymatic activity, lung inflammation, and cystic fibrosis. *Am J Respir Crit Care Med.* 2012;186:162-169.
15. Baugh JA, Chitnis S, Donnelly SC, et al. A functional promoter polymorphism in the macrophage migration inhibitory factor (MIF) gene associated with disease severity in rheumatoid arthritis. *Genes Immun.* 2002;3:170-176.
16. Lefebvre JS, Maue AC, Eaton SM, Lanthier PA, Tighe M, Haynes L. The aged microenvironment contributes to the age-related functional defects of CD4 T cells in mice. *Aging Cell.* 2012;11:732-740.
17. Wirtz TH, Tillmann S, Strussmann T, et al. Platelet-derived MIF: a novel platelet chemokine with distinct recruitment properties. *Atherosclerosis.* 2015;239:1-10.
18. Bernhagen J, Krohn R, Lue H, et al. MIF is a noncognate ligand of CXC chemokine receptors in inflammatory and atherogenic cell recruitment. *Nat Med.* 2007;13:587-596.
19. Asare Y, Schmitt M, Bernhagen J. The vascular biology of macrophage migration inhibitory factor (MIF). Expression and effects in inflammation, atherogenesis and angiogenesis. *Thromb Haemost.* 2013;109:391-398.
20. Schober A, Bernhagen J, Thiele M, et al. Stabilization of atherosclerotic plaques by blockade of macrophage migration inhibitory factor after vascular injury in apolipoprotein E-deficient mice. *Circulation.* 2004;109:380-385.
21. Pan JH, Sukhova GK, Yang JT, et al. Macrophage migration inhibitory factor deficiency impairs atherosclerosis in low-density lipoprotein receptor-deficient mice. *Circulation.* 2004;109:3149-3153.
22. Burger-Kentischer A, Gobel H, Kleemann R, et al. Reduction of the aortic inflammatory response in spontaneous atherosclerosis by blockade of macrophage migration inhibitory factor (MIF). *Atherosclerosis.* 2006;184:28-38.
23. Schmitz C, Noels H, El Bounkari O, et al. Mif-deficiency favors an atheroprotective autoantibody phenotype in atherosclerosis. *FASEB J.* 2018;32:4428-4443.
24. Nakashima Y, Plump AS, Raines EW, Breslow JL, Ross R. ApoE-deficient mice develop lesions of all phases of atherosclerosis throughout the arterial tree. *Arterioscler Thromb Vasc Biol.* 1994;14:133-140.
25. Fox J, Barthold S, Davisson M, Newcomer C, Quimby F, Smith A. *The Mouse in Biomedical Research.* Elsevier; 2007.
26. Liberale L, Montecucco F, Tardif JC, Libby P, Camici GG. Inflamm-aging: the role of inflammation in age-dependent cardiovascular disease. *Eur Heart J.* 2020;41:2974-2982.
27. Mohanta SK, Yin C, Peng L, et al. Artery tertiary lymphoid organs contribute to innate and adaptive immune responses in advanced mouse atherosclerosis. *Circ Res.* 2014;114:1772-1787.
28. Yin C, Mohanta SK, Srikakulapu P, Weber C, Habenicht AJ. Artery tertiary lymphoid organs: powerhouses of atherosclerosis immunity. *Front Immunol.* 2016;7:387.
29. Mohanta SK, Peng L, Li Y, et al. Neuroimmune cardiovascular interfaces control atherosclerosis. *Nature.* 2022;605:152-159.
30. Akhavanpoor M, Gleissner CA, Akhavanpoor H, et al. Adventitial tertiary lymphoid organ classification in human atherosclerosis. *Cardiovasc Pathol.* 2018;32:8-14.
31. Fingerle-Rowson G, Petrenko O, Metz CN, et al. The p53-dependent effects of macrophage migration inhibitory factor revealed by gene targeting. *Proc Natl Acad Sci U S A.* 2003;100:9354-9359.
32. Asare Y, Ommer M, Azombo FA, et al. Inhibition of atherogenesis by the COP9 signalosome subunit 5 in vivo. *Proc Natl Acad Sci U S A.* 2017;114:E2766-E2775.
33. Schlepckow K, Monroe KM, Kleinberger G, et al. Enhancing protective microglial activities with a dual function TREM2 antibody to the stalk region. *EMBO Mol Med.* 2020;12:e11227.
34. Picelli S, Bjorklund AK, Faridani OR, Sagasser S, Winberg G, Sandberg R. Smart-seq2 for sensitive full-length transcriptome profiling in single cells. *Nat Methods.* 2013;10:1096-1098.
35. Safaiyan S, Besson-Girard S, Kaya T, et al. White matter aging drives microglial diversity. *Neuron.* 2021;109:1100-1117.e1110.
36. Dobin A, Davis CA, Schlesinger F, et al. STAR: ultrafast universal RNA-seq aligner. *Bioinformatics.* 2013;29:15-21.
37. Huber W, von Heydebreck A, Sultmann H, Poustka A, Vingron M. Variance stabilization applied to microarray data calibration and to the quantification of differential expression. *Bioinformatics.* 2002;18(suppl 1):S96-S104.
38. Love MI, Huber W, Anders S. Moderated estimation of fold change and dispersion for RNA-seq data with DESeq2. *Genome Biol.* 2014;15:550.
39. Chen Z, Sakuma M, Zago AC, et al. Evidence for a role of macrophage migration inhibitory factor in vascular disease. *Arterioscler Thromb Vasc Biol.* 2004;24:709-714.
40. Ma H, Wang J, Thomas DP, et al. Impaired macrophage migration inhibitory factor-AMP-activated protein kinase activation and ischemic recovery in the senescent heart. *Circulation.* 2010;122:282-292.
41. Cochain C, Vafadarnejad E, Arampatzi P, et al. Single-cell RNA-seq reveals the transcriptional landscape and heterogeneity of aortic macrophages in murine atherosclerosis. *Circ Res.* 2018;122:1661-1674.
42. Willemsen L, de Winther MP. Macrophage subsets in atherosclerosis as defined by single-cell technologies. *J Pathol.* 2020;250:705-714.
43. Kim K, Shim D, Lee JS, et al. Transcriptome analysis reveals nonfoamy rather than foamy plaque macrophages are proinflammatory in atherosclerotic murine models. *Circ Res.* 2018;123:1127-1142.
44. Yang H, Galea A, Sytnyk V, Crossley M. Controlling the size of lipid droplets: lipid and protein factors. *Curr Opin Cell Biol.* 2012;24:509-516.

45. Buers I, Hofnagel O, Ruebel A, Severs NJ, Robenek H. Lipid droplet associated proteins: an emerging role in atherogenesis. *Histol Histopathol.* 2011;26:631-642.
46. Liu SL, Li YH, Shi GY, Jiang MJ, Chang JH, Wu HL. The effect of statin on the aortic gene expression profiling. *Int J Cardiol.* 2007;114:71-77.
47. Menendez JA, Lupu R. Fatty acid synthase and the lipogenic phenotype in cancer pathogenesis. *Nat Rev Cancer.* 2007;7:763-777.
48. Wu J, Wang C, Li S, et al. Thyroid hormone-responsive SPOT 14 homolog promotes hepatic lipogenesis, and its expression is regulated by liver X receptor alpha through a sterol regulatory element-binding protein 1c-dependent mechanism in mice. *Hepatology.* 2013;58:617-628.
49. Domschke G, Linden F, Pawig L, et al. Systematic RNA-interference in primary human monocyte-derived macrophages: a high-throughput platform to study foam cell formation. *Sci Rep.* 2018;8:10516.
50. Brown MS, Kovanen PT, Goldstein JL. Regulation of plasma cholesterol by lipoprotein receptors. *Science.* 1981;212:628-635.
51. Sokeechand BSH, Trigatti BL. Un-JAMming atherosclerotic arteries: JAM-L as a target to attenuate plaque development. *Clin Sci (Lond).* 2019;133:1581-1585.
52. Steffensen LB, Rasmussen LM. A role for collagen type IV in cardiovascular disease? *Am J Physiol Heart Circ Physiol.* 2018;315:H610-H625.
53. Atsumi T, Singh R, Sabharwal L, et al. Inflammation amplifier, a new paradigm in cancer biology. *Cancer Res.* 2014;74:8-14.
54. Lelios I, Cansever D, Utz SG, Mildenerberger W, Stifter SA, Greter M. Emerging roles of IL-34 in health and disease. *J Exp Med.* 2020;217:e20190290.
55. Campbell KA, Lipinski MJ, Doran AC, Skafien MD, Fuster V, McNamara CA. Lymphocytes and the adventitial immune response in atherosclerosis. *Circ Res.* 2012;110:889-900.
56. Hu D, Mohanta SK, Yin C, et al. Artery tertiary lymphoid organs control aorta immunity and protect against atherosclerosis via vascular smooth muscle cell lymphotoxin beta receptors. *Immunity.* 2015;42:1100-1115.
57. Srikakulapu P, Hu D, Yin C, et al. Artery tertiary lymphoid organs control multilayered territorialized atherosclerosis B-cell responses in aged ApoE^{-/-} mice. *Arterioscler Thromb Vasc Biol.* 2016;36:1174-1185.
58. Tsiantoulas D, Diehl CJ, Witztum JL, Binder CJ. B cells and humoral immunity in atherosclerosis. *Circ Res.* 2014;114:1743-1756.
59. Tyrrell DJ, Goldstein DR. Ageing and atherosclerosis: vascular intrinsic and extrinsic factors and potential role of IL-6. *Nat Rev Cardiol.* 2021;18:58-68.
60. Liu D, Richardson G, Benli FM, et al. Inflammageing in the cardiovascular system: mechanisms, emerging targets, and novel therapeutic strategies. *Clin Sci (Lond).* 2020;134:2243-2262.
61. Smykiewicz P, Segiet A, Keag M, Zera T. Proinflammatory cytokines and ageing of the cardiovascular-renal system. *Mech Ageing Dev.* 2018;175:35-45.
62. Rammos C, Hendgen-Cotta UB, Pohl J, et al. Modulation of circulating macrophage migration inhibitory factor in the elderly. *Biomed Res Int* 2014;2014:582586.
63. Rammos C, Hendgen-Cotta UB, Deenen R, et al. Age-related vascular gene expression profiling in mice. *Mech Ageing Dev.* 2014;135:15-23.
64. Zhao X, Gao M, He J, et al. Perilipin1 deficiency in whole body or bone marrow-derived cells attenuates lesions in atherosclerosis-prone mice. *PLoS ONE.* 2015;10:e0123738.
65. Trott DW, Henson GD, Ho MHT, Allison SA, Lesniewski LA, Donato AJ. Age-related arterial immune cell infiltration in mice is attenuated by caloric restriction or voluntary exercise. *Exp Gerontol.* 2018;109:99-107.
66. Trott DW, Fadel PJ. Inflammation as a mediator of arterial ageing. *Exp Physiol.* 2019;104:1455-1471.
67. Du W, Wong C, Song Y, et al. Age-associated vascular inflammation promotes monocytosis during atherogenesis. *Ageing Cell.* 2016;15:766-777.
68. Eleftheriadis T, Antoniadi G, Liakopoulos V, et al. Perilipin-1 in hemodialyzed patients: association with history of coronary heart disease and lipid profile. *Ther Apher Dial.* 2012;16:355-360.
69. Fan Q, Yan X, Zhang H, et al. IL-34 is associated with the presence and severity of renal dysfunction and coronary artery disease in patients with heart failure. *Sci Rep.* 2016;6:39324.
70. Liu Q, Fan J, Bai J, et al. IL-34 promotes foam cell formation by enhancing CD36 expression through p38 MAPK pathway. *Sci Rep.* 2018;8:17347.
71. Mitchell RA, Liao H, Chesney J, et al. Macrophage migration inhibitory factor (MIF) sustains macrophage proinflammatory function by inhibiting p53: regulatory role in the innate immune response. *Proc Natl Acad Sci U S A.* 2002;99:345-350.
72. Aw D, Hilliard L, Nishikawa Y, Cadman ET, Lawrence RA, Palmer DB. Disorganization of the splenic microanatomy in ageing mice. *Immunology.* 2016;148:92-101.
73. Masters AR, Jellison ER, Puddington L, Khanna KM, Haynes L. Attrition of T cell zone fibroblastic reticular cell number and function in aged spleens. *ImmunoHorizons.* 2018;2:155-163.
74. Saigusa R, Winkels H, Ley K. T cell subsets and functions in atherosclerosis. *Nat Rev Cardiol.* 2020;17:387-401.
75. Larbi A, Dupuis G, Khalil A, Douziech N, Fortin C, Fulop T Jr. Differential role of lipid rafts in the functions of CD4+ and CD8+ human T lymphocytes with aging. *Cell Signal.* 2006;18:1017-1030.
76. Bazioti V, La Rose AM, Maassen S, et al. T cell cholesterol efflux suppresses apoptosis and senescence and increases atherosclerosis in middle aged mice. *Nat Commun.* 2022;13:3799.
77. Tomsig JL, Creutz CE. Copines: a ubiquitous family of Ca(2+)-dependent phospholipid-binding proteins. *Cell Mol Life Sci.* 2002;59:1467-1477.
78. Toubal A, Nel I, Lotersztajn S, Lehuen A. Mucosal-associated invariant T cells and disease. *Nat Rev Immunol.* 2019;19:643-657.
79. Novikova OA, Nazarkina ZK, Cherepanova AV, et al. Isolation, culturing and gene expression profiling of inner mass cells from stable and vulnerable carotid atherosclerotic plaques. *PLoS ONE.* 2019;14:e0218892.
80. Allahverdian S, Chaabane C, Boukais K, Francis GA, Bochaton-Piallat ML. Smooth muscle cell fate and plasticity in atherosclerosis. *Cardiovasc Res.* 2018;114:540-550.
81. Fan Y, Zhang J, Chen CY, et al. Macrophage migration inhibitory factor triggers vascular smooth muscle cell dedifferentiation by a p68-serum response factor axis. *Cardiovasc Res.* 2017;113:519-530.
82. Moos MP, John N, Grabner R, et al. The lamina adventitia is the major site of immune cell accumulation in standard chow-fed

- apolipoprotein E-deficient mice. *Arterioscler Thromb Vasc Biol.* 2005;25:2386-2391.
83. Stranford S, Ruddle NH. Follicular dendritic cells, conduits, lymphatic vessels, and high endothelial venules in tertiary lymphoid organs: parallels with lymph node stroma. *Front Immunol.* 2012;3:350.
84. Kyaw T, Tay C, Krishnamurthi S, et al. B1a B lymphocytes are atheroprotective by secreting natural IgM that increases IgM deposits and reduces necrotic cores in atherosclerotic lesions. *Circ Res.* 2011;109:830-840.
85. Rosenfeld SM, Perry HM, Gonen A, et al. B-1b cells secrete atheroprotective IgM and attenuate atherosclerosis. *Circ Res.* 2015;117:e28-e39.
86. Nosalski R, Guzik TJ. Perivascular adipose tissue inflammation in vascular disease. *Brit J Pharmacol.* 2017;174:3496-3513.
87. Ahmadiéh S, Kim HW, Weintraub NL. Potential role of perivascular adipose tissue in modulating atherosclerosis. *Clin Sci (Lond).* 2020;134:3-13.
88. Camino T, Lago-Baameiro N, Sueiro A, et al. Brown adipose tissue sheds extracellular vesicles that carry potential biomarkers of metabolic and thermogenesis activity which are affected by high fat diet intervention. *Int J Mol Sci.* 2022;23:10826.
89. Ridker PM, Everett BM, Thuren T, et al. Antiinflammatory therapy with canakinumab for atherosclerotic disease. *N Engl J Med.* 2017;377:1119-1131.
90. Krammer C, Kontos C, Dewor M, et al. A MIF-derived cyclopeptide that inhibits MIF binding and atherogenic signaling via the chemokine receptor CXCR2. *Chembiochem.* 2021;22:1012-1019.
91. Kontos C, El Bounkari O, Krammer C, et al. Designed CXCR4 mimic acts as a soluble chemokine receptor that blocks atherogenic inflammation by agonist-specific targeting. *Nat Commun.* 2020;11:5981.
92. Merk M, Zierow S, Leng L, et al. The D-dopachrome tautomerase (DDT) gene product is a cytokine and functional homolog of macrophage migration inhibitory factor (MIF). *Proc Natl Acad Sci U S A.* 2011;108:E577-E585.
93. Kim BS, Tilstam PV, Arnke K, et al. Differential regulation of macrophage activation by the MIF cytokine superfamily members MIF and MIF-2 in adipose tissue during endotoxemia. *FASEB J.* 2020;34:4219-4233.
94. El Bounkari O, Zan C, Wagner J, et al. MIF-2/D-DT is an atypical atherogenic chemokine that promotes advanced atherosclerosis and hepatic lipogenesis. *bioRxiv.* 2021. doi:[10.1101/2021.12.28.474328](https://doi.org/10.1101/2021.12.28.474328)

SUPPORTING INFORMATION

Additional supporting information can be found online in the Supporting Information section at the end of this article.

How to cite this article: Krammer C, Yang B, Reichl S, et al. Pathways linking aging and atheroprotection in *Mif*-deficient atherosclerotic mice. *The FASEB Journal.* 2023;37:e22752. doi:[10.1096/fj.202200056R](https://doi.org/10.1096/fj.202200056R)